Draft version November 30, 2005
Preprint typeset using LaTeX style emulateapj

COMPACT OBJECT MODELING WITH THE STARTRACK POPULATION SYNTHESIS CODE

Krzysztof Belczynski[1,2], Vassiliki Kalogera[3], Frederic A. Rasio [3], Ronald E. Taam[3], Andreas Zezas[4], Tomasz Bulik[5], Thomas J. Maccarone[6,7] and Natalia Ivanova[8]

[1] New Mexico State University, Dept of Astronomy, 1320 Frenger Mall, Las Cruces, NM 88003
[2] Tombaugh Fellow
[3] Northwestern University, Dept of Physics & Astronomy, 2145 Sheridan Rd, Evanston, IL 60208
[4]Harvard–Smithsonian Center for Astrophysics, 60 Garden St, Cambridge, MA 02138;
[5] Nicolaus Copernicus Astronomical Center, Bartycka 18, 00-716 Warszawa, Poland;
[6] Astronomical Institute Anton Pannekoek, University of Amsterdam, Kruislaan 403, 1098 SJ, Amsterdam, The Netherlands
[7] School of Physics and Astronomy, University of Southampton, Southampton, Hampshire, SO17 1BJ, United Kingdom
[8] Canadian Institute for Theoretical Astrophysics, University of Toronto, 60 St. George, Toronto, ON M5S 3H8, Canada
kbelczyn@nmsu.edu, vicky, rasio, r-taam@northwestern.edu, azezas@head-cfa.cfa.harvard.edu, bulik@camk.edu.pl, tjm@phys.soton.ac.uk, nata@cita.utoronto.ca

Draft version November 30, 2005

ABSTRACT

We present a comprehensive description of the population synthesis code StarTrack. The original code has been significantly modified and updated. Special emphasis is placed here on processes leading to the formation and further evolution of compact objects (white dwarfs, neutron stars, and black holes). Both single and binary star populations are considered. The code now incorporates detailed calculations of all mass-transfer phases, a full implementation of orbital evolution due to tides, as well as the most recent estimates of magnetic braking. This updated version of StarTrack can be used for a wide variety of problems, with relevance to many current and planned observatories, e.g., studies of X-ray binaries (Chandra, XMM-Newton), gravitational radiation sources (LIGO, LISA), and gamma-ray burst progenitors (HETE-II, Swift). The code has already been used in studies of Galactic and extra-galactic X-ray binary populations, black holes in young star clusters, Type Ia supernova progenitors, and double compact object populations. Here we describe in detail the input physics, we present the code calibration and tests, and we outline our current studies in the context of X-ray binary populations.

Subject headings: binaries: close — stars: evolution — stars: white dwarfs, neutron — black hole physics — X-rays: binaries

1. INTRODUCTION

The StarTrack population synthesis code was initially developed for the study of double compact object mergers in the context of gamma-ray burst (GRB) progenitors (Belczynski, Bulik & Rudak 2002b) and gravitational radiation inspiral sources (Belczynski, Kalogera & Bulik 2002c, hereafter BKB02). StarTrack has undergone major updates and revisions in the last few years. With this code we are able to evolve isolated (not dynamically interacting) single stars and binaries for a wide range of initial conditions. The input physics incorporates our latest knowledge of processes governing stellar evolution, while the most uncertain aspects are parameterized to allow for systematic error analysis. During the code development, special emphasis was placed on the compact object populations: white dwarfs (WDs), neutron stars (NSs), and black holes (BHs). The input physics currently includes all major processes important for the formation and evolution of compact objects. Among other things we have developed fast procedures to treat and diagnose various types of mass transfer episodes (including phases unstable on the thermal time scale and dynamically unstable mass transfer leading to common envelopes). We also compute tidal effects on orbital evolution, angular momentum losses due to magnetic braking and gravitational radiation, as well as mass loss from stellar winds and during mass transfer phases. Rejuvenation of binary components is taken into account. The full orbital evolution of binaries is also computed, including angular momentum and mass loss. Supernovae (SNe) and compact object formation are also treated in detail.

The new version of StarTrack presented here has already been tested and used in many applications. Belczynski & Taam (2004a) studied the formation of ultrashort period X-ray binaries and they also demonstrated that the faint X-ray Galactic Center population can neither be explained by quiescent NS/BH transients nor by hard/faint wind-fed sources (Belczynski & Taam 2004b). Belczynski, Sadowski & Rasio (2004b) and Belczynski et al. (2005c) developed a comprehensive description of young BH populations, which can also provide realistic initial conditions for the dynamical modeling of BHs in star clusters. Belczynski et al. (2004a) derived for the first time a synthetic X-ray luminosity function which agrees with *Chandra* observations of NGC 1659, and Sepinsky, Kalogera, & Belczynski (2005) explored the numbers and spatial distribution of X-ray binaries formed in young star clusters. Belczynski, Bulik & Ruiter (2005b) tested different models of Type Ia SN progenitors, arriving at the conclusion that the double degenerate scenario most easily reproduces the observed delay times between star formation and Type Ia SNe. Belczynski et al. (2005a) used StarTrack to study the gravitational radiation signal from the Galactic population of double WDs. Nutzman et al. (2004), O'Shaughnessy et al. (2005a,b,c), and Ihm, Kalogera, & Belczynski (2005) studied binary compact object popu-

lations and derived merger rates and detection rates by ground-based interferometers; they also examined BH spin magnitudes and studied the eccentricities of double neutron stars. `StarTrack` was also incorporated into a simple stellar dynamics code, allowing the study of the effects of dynamical interactions on binary populations in dense star clusters. In that form it has been used for the study of binary fractions in globular clusters (Ivanova et al. 2005) and an investigation of intermediate-mass BHs in clusters and their connection to ultra-luminous X-ray sources (Blecha et al. 2005).

Among other things `StarTrack` has been adapted for the study of accretion powered X-ray binaries (XRBs). In forthcoming papers we will present the synthetic populations of XRBs formed in different stellar environments. We will start with young starburst galaxies, and move on to spiral and, eventually, old elliptical galaxies. In the next stage it will be possible to compare the models with rapidly improving observations of various X-ray point source populations. This will offer a new perspective to the study of several uncertain aspects of binary evolution leading to the formation of XRBs. It may also result in an independent diagnostic of star formation rates for nearby galaxies, since both the numbers and properties of XRBs are directly connected to the star formation history (see e.g., Grimm, Gilfanov & Sunyaev 2003; Gilfanov 2004; Kim & Fabbiano 2004; Belczynski et al. 2006, in preparation).

In this paper we provide a detailed description of the current version of `StarTrack`, and we present the results of a number of tests. We describe the implementations of single star evolution in § 2, binary orbit evolution in § 3, stellar wind mass loss/accretion in § 4, Roche lobe overflow calculations in § 5, spatial velocities in § 6, and the assumed distributions of initial parameters in § 7. In § 8 we discuss the validity of various input physics assumptions, and we compare `StarTrack` calculations with detailed evolutionary models and with various observations. Section § 9 is dedicated to the discussion of X-ray binary modeling. In § 10 we conclude with a short summary.

2. SINGLE STELLAR EVOLUTION

In all subsequent sections we use units of $M_\odot$ for mass, $R_\odot$ for orbital separations and stellar radii, Myr for time, $L_\odot$ for bolometric luminosity, unless specified otherwise. We use R and M to denote stellar radius and mass, while a, e represent the binary orbital parameters: semi-major axis and eccentricity, respectively. Index $i = 1, 2$ is used to mark the binary components (or single stars for consistency), or to denote an accretor and a donor in mass transfer calculations: $i = \mathrm{acc}, \mathrm{don}$. Roche lobe parameters are indexed with "lob". The initially more massive (at Zero Age Main Sequence) binary component is referred to as primary, while its companion as secondary.

2.1. *Overview*

The evolution of single stars and non-interacting binary components have remained mostly unchanged since the last published description of the code (BKB02) and therefore we only give a brief outline here. However, we do point out the new additions and reiterate the modifications to the original formulae which were used as the base for the implementation of single star evolution in `StarTrack`.

To evolve single stars from the Zero Age Main Sequence (ZAMS) until remnant formation (WD, NS, BH, or a remnant-less supernova) we employ the analytic formulae of Hurley, Pols & Tout (2000). Each star is followed along an evolutionary track specific for its initial mass and metallicity. Various wind mass loss rates that vary with the stellar evolutionary stage are incorporated into the code and their effect on stellar evolution is taken into account. Once the remnant is formed, we terminate the calculations but keep track of the numbers, properties and formation times of a given type of remnant.

2.2. *Stellar types*

We follow Hurley et al. (2000) to denote different stages of stellar evolution with an integer $K_\mathrm{i} = 1..n$, where
0 – Main Sequence (MS) $M \leq 0.7$ M$_\odot$
1 – MS $M > 0.7$ M$_\odot$
2 – Hertzsprung Gap (HG)
3 – Red Giant Branch (RG)
4 – Core Helium Burning (CHeB)
5 – Early Asymptotic Giant Branch (EAGB)
6 – Thermally Pulsing AGB (TPAGB)
7 – Helium Main Sequence (HeMS)
8 – Helium Hertzsprung Gap (HeHG)
9 – Helium Giant Branch (HeGB)
10 – Helium White Dwarf (He WD)
11 – Carbon/Oxygen White Dwarf (CO WD)
12 – Oxygen/Neon White Dwarf (ONe WD)
13 – Neutron Star (NS)
14 – Black Hole (BH)
15 – massless remnant (after SN Ia explosion)
16 – Hydrogen White Dwarf (H WD)
17 – Hybrid White Dwarf (Hyb WD)
In addition to the star types introduced and coded by the numbers $K_\mathrm{i} = 1...15$ in the original Hurley et al. (2000) formulae, we have introduced two new stellar types $K_\mathrm{i} = 16, 17$. $K_\mathrm{i} = 16$ denotes a H-rich white dwarf. Only main sequence stars less massive than about 0.7 M$_\odot$ can produce such a H-rich remnant through mass loss in a close binary system. These low-mass stars do not process a significant amount of hydrogen into helium in their cores (even in a Hubble time) and once their mass is stripped below the hydrogen burning limit (close to ~ 0.08 M$_\odot$) they become degenerate H-rich white dwarfs. These stars, although not frequently encountered in population synthesis, may become donors in the shortest-period interacting binaries. $K_\mathrm{i} = 17$ denotes a hybrid white dwarf, with a carbon-oxygen-helium mixture in the core and a helium envelope. These objects are the remnants of Helium-rich main sequence stars ($K_\mathrm{i} = 7$) which are stripped of mass below 0.35 M$_\odot$ during Roche lobe overflow (RLOF). At that point, thermonuclear reactions stop and the star becomes degenerate (eg., Savonije, de Kool & van den Heuvel 1986).

2.3. *Modifications*

Several major changes to the original Hurley et al. (2000) formulae have been implemented within `StarTrack`.

2.3.1. *Compact object masses*

The remnant masses of neutron stars and black holes are also calculated in a different way than originally suggested

by Hurley et al. (2000). We determine the mass of a remnant using the information on the final CO and FeNi core masses, combined with the knowledge of the initial mass of the star. The effects of material fallback (ejected initially in the SN explosion) during the star's final collapse are included. For the most massive stars we also allow for the possibility of a silent collapse (no supernova explosion) and direct BH formation. The resulting remnant mass spectrum covers a wide range of masses. In particular, it was found that single stars may form BHs up to ~ 12 M$_\odot$ for solar metallicity ($Z = 0.02$) and ~ 30 M$_\odot$ for lower metallicities ($Z = 0.001 - 0.0001$), which is in agreement with the current observations of most massive BHs in X-ray transients. The details of the remnant mass calculations were presented and discussed in BKB02 (see their § 2.1.3) and the dependence of remnant mass on metallicity was presented in Belczynski et al. (2004b).

2.3.2. *Wind mass loss*

The compilation of stellar winds mass loss rates presented in Hurley et al. (2000) has been expanded to include mass loss from low- and intermediate-mass main sequence stars. We have adopted the formulae of Nieuwenhuijzen & de Jager (1990) to calculate the mass loss rates for main sequence stars below ~ 8 M$_\odot$. Although the mass loss from these stars is not large enough to significantly alter the evolution of a mass–losing star, it may play an important role in the formation and evolution of wind-accreting close binaries. Even with small mass transfer rates characteristic for the low- and intermediate-mass main sequence stars, the X-ray luminosities for accreting BHs and NSs are high enough to be detected in deep Chandra exposures. A number of faint point X-ray sources were discovered in the Galactic center with deep exposures (Wang, Gotthelf & Lang 2002; Muno et al. 2003), some of which may be explained in terms of wind-fed close binaries (Pfahl, Rappaport & Podsiadlowski 2002a; Bleach 2002; Willems & Kolb 2003; Belczynski & Taam 2004b).

2.3.3. *Rotational velocities*

A compilation of updated observational data on rotational velocities is used to initiate the stellar spins on the ZAMS. The spin evolution is followed as detailed here for single stars and in § 3 for binary components. In order to obtain a functional form of the relation of the equatorial rotational velocity and stellar mass, we used the compilation of rotational velocities of Stauffer & Hartmann (1986) for stars in open clusters. The difference between cluster and field stars is quite small for massive stars (with a maximum difference of $\sim 10\%$ for intermediate B-type stars), but can be as high as 40% for stars later than F-type, with field stars having systematically lower rotational velocities.

The mean rotational velocity $\overline{\mathrm{v}}_{\mathrm{rot}}$ was determined from the projected velocity ($\mathrm{v}_{\mathrm{rot}} \sin \mathrm{i}$) assuming a random distribution of angles with $\sin \mathrm{i} = \pi/4$. We fitted $\overline{\mathrm{v}}_{\mathrm{rot}}$ as a function of stellar mass, and we obtained the following empirical functional form

$$\overline{\mathrm{v}}_{\mathrm{rot}} = \begin{cases} \frac{10.0\, M_{\mathrm{i}}^{-\alpha_1}}{c + M_{\mathrm{i}}^{-\beta_1}} & if\ M_{\mathrm{i}} > M_o \\ \frac{13.32\, M_{\mathrm{i}}^{-\alpha_2}}{c + M_{\mathrm{i}}^{-\beta_1}} & if\ M_{\mathrm{i}} \leq M_o \end{cases} \quad (1)$$

where, $\alpha_1 = -0.035^{+0.06}_{-0.31}$, $\alpha_2 = 0.12^{+0.09}_{-0.04}$, $\beta_1 = 7.95^{+0.33}_{-0.31}$ and $M_o = 6.35^{+6.5}_{-2.1}$ (errors are at the 1 σ level). We stress that this is only an empirical functional form of the equatorial rotational velocity as a function of stellar mass. In Fig 1 we present the observational data from Stauffer & Hartmann (1986), together with the best fit function. In the bottom panel of this figure we also show the ratio of the Stauffer & Hartmann (1986) data and the model.

The spin angular momentum of a star may be expressed as

$$J_{\mathrm{i,spin}} = I_{\mathrm{i}} \omega_{\mathrm{i}} = k_{\mathrm{i}} M_{\mathrm{i}} R_{\mathrm{i}}^2 \omega_{\mathrm{i}} \quad (2)$$

where, $\omega_{\mathrm{i}} = \overline{\mathrm{v}}_{\mathrm{rot}}/\mathrm{R}_{\mathrm{i}}$ is the angular rotational velocity and the coefficient k_{i} varies as the star evolves and its internal structure changes (e.g., it is 2/5 for a solid sphere and 2/3 for a spherical shell). Following Hurley et al. (2000) we consider two structural components for each star: a core and an envelope. The spins of these two components may decouple in the course of evolution, although we keep them coupled in our standard model calculations. The spin angular momentum of a star is then

$$J_{\mathrm{i,spin}} = [k_{\mathrm{i,env}}(M_{\mathrm{i}} - M_{\mathrm{i,c}}) R_{\mathrm{i}}^2 + k_{\mathrm{i,core}} M_{\mathrm{i,c}} R_{\mathrm{i,c}}^2] \omega_{\mathrm{i}} \quad (3)$$

We use different values than Hurley at al. (2000) for the internal structure coefficient k_{i}. For stars with no clear core-envelope structure ($K_{\mathrm{i}} = 0, 1, 7, 10, 11, 12, 13, 14, 16, 17$) we use simple polytropic models (e.g., Lai, Rasio & Shapiro 1993) with $n = 1.5$ and $n = 3$ for low-mass and high-mass objects, respectively, giving

$$k_{\mathrm{i,env}} = \begin{cases} 0.205 & M_{\mathrm{i}} < 1\ \mathrm{M}_\odot \\ 0.075 & M_{\mathrm{i}} \geq 1\ \mathrm{M}_\odot \end{cases} \quad k_{\mathrm{i,core}} = 0 \quad (4)$$

For giants with a clear separation between core and envelope ($K_{\mathrm{i}} = 2, 3, 4, 5, 6, 8, 9$) we use detailed models of giant envelopes (Hurley et al. 2000) and for the core we apply a polytropic model with $n = 1.5$ to obtain

$$k_{\mathrm{i,env}} = 0.1, \quad k_{\mathrm{i,core}} = 0.205 \quad (5)$$

Conservation of the spin angular momentum of a star is used then to determine its rotational velocity. Additional momentum losses from magnetic braking (see § 3.2) are also taken into account.

2.3.4. *Convective/Radiative envelopes*

Stars with convective and radiative envelopes respond differently to various physical processes (e.g., magnetic braking, tidal interactions or mass loss). Stars that have a significant convective envelope are: low-mass H-rich MS stars ($K_{\mathrm{i}} = 0, 1$) within the mass range of $0.35\ \mathrm{M}_\odot - M_{\mathrm{ms,conv}}$, where $M_{\mathrm{ms,conv}}$ is the maximum mass for a MS star to develop a convective envelope; giant-like stars ($K_{\mathrm{i}} = 2, 3, 5, 6, 8, 9$) independent of their mass; low- and intermediate-mass core helium burning stars ($K_{\mathrm{i}} = 4$ with $M_{\mathrm{i}} < 7\ \mathrm{M}_\odot$); and evolved low-mass Helium stars ($K_{\mathrm{i}} = 9$) below $M_{\mathrm{he,conv}} = 3.0\ \mathrm{M}_\odot$. MS stars with masses below ~ 0.35 are fully convective. The value of $M_{\mathrm{ms,conv}}$) depends strongly on metallicity

$$M_{\mathrm{ms,conv}} = \begin{cases} 1.25 & Z \geq 0.02 \\ -1532 Z^2 + 55.73 Z + 0.747 & 0.001 < Z < 0.02 \\ 0.8 & Z \leq 0.001 \end{cases} \quad (6)$$

Values of $M_{\rm ms,conv}$ in metallicity range $Z = 0.001 - 0.02$ are obtained from a fit to the detailed evolutionary calculations (Ivanova 2006). All other stars are assumed to have radiative envelopes.

2.3.5. *Helium star evolution*

We assume that low-mass evolved Helium stars ($K_{\rm i} = 9$) below $M_{\rm he,conv} = 3.0$ M$_\odot$ (as opposed to 2.2 M$_\odot$ in Hurley et al. 2000) expand and form deep convective envelopes in the late stages of evolution (e.g., Ivanova et al. 2003; Dewi & Pols 2003). Helium stars with convective envelopes are subject to strong tidal interactions (convective tides as opposed to radiative damping, see § 3.3), and if found in an interacting binary, they may alter significantly the fate of a given system. All helium stars ($K_{\rm i} = 7, 8, 9$) may be subject to stable RLOF. However, in dynamically unstable cases we assume a binary component merger in the case of a HeMS donor ($K_{\rm i} = 7$) or we follow a given system through a CE phase for evolved He star donors ($K_{\rm i} = 8, 9$ and test whether the system survives or merges. The examination of RLOF stability and development of dynamical instability are described in detail in § 5).

The treatment of helium stars is important, among other things, in later stages of evolution leading to double neutron star formation. The immediate consequences, leading to the formation of a new class of close double neutron stars, were discussed in Belczynski & Kalogera (2001), Belczynski, Bulik & Kalogera (2002a) and Ivanova et al. (2003). Due to significant updates of the code and new observational results on short GRBs with double neutron stars suggested as their progenitors (e.g., Fox et al. 2005) new `StarTrack` calculations relevant to the double neutron star formation are underway.

3. BINARY ORBITAL EVOLUTION

Throughout the course of binary evolution we track the changes in orbital properties. A number of physical processes may be responsible for these changes. In the general case of eccentric orbits we numerically integrate a set of four differential equations describing the evolution of orbital separation, eccentricity and component spins, which depend on tidal interactions as well as angular momentum losses associated with magnetic braking, gravitational radiation and stellar wind mass losses. For circular orbits with synchronized components, we can obtain an exact solution for the change of orbital separation using conservation of angular momentum. Losses of angular momentum and/or mass associated with RLOF events, magnetic braking and gravitational radiation are taken into account. We assume that any system entering RLOF becomes circularized and synchronized (if it had not already reached this equilibrium state before RLOF). For systems which have not been circularized and synchronized before entering RLOF there might be substantial mass loss (e.g., Hut & Paczynski 1984), and this is not taken into account in our calculations. Violent processes like SN explosions or common envelope phases are taken into account in binary orbital evolution. Also nuclear evolution of components (expansion/contraction affecting stellar spins) is considered. In what follows we describe the elements used to calculate the orbital evolution.

The orbital angular momentum of the binary and its mean angular velocity are expressed as

$$J_{\rm orb} = \frac{M_1 M_2 \sqrt{aG(M_1+M_2)}}{M_1+M_2}\sqrt{1-e^2} \qquad (7)$$

$$w_{\rm worb} = \sqrt{G(M_1+M_2)}a^{-1.5} \qquad (8)$$

where G is the gravitational constant.

3.1. *Gravitational radiation*

Binary angular momentum loss due to gravitational radiation is estimated for any type of binary following Peters (1964)

$$dJ_{\rm gr}/\,dt = -\frac{32}{5}\frac{G^{\frac{7}{2}}{M_1}^2{M_2}^2\sqrt{M_1+M_2}}{c^5 a^{\frac{7}{2}}(1-e^2)^2}(1+\frac{7}{8}e^2) \qquad (9)$$

where, c is the speed of light.

3.2. *Magnetic Braking*

Three different prescriptions for magnetic braking are incorporated within the `StarTrack` code and may be used interchangingly for parameter studies. In what follows we provide a detailed description of the specific braking laws adopted.

Magnetic braking is applied for stars with a significant convective envelope, i.e., for low-mass H-rich MS stars, H-rich giant-like stars and low- and intermediate-mass CHeB stars (see § 2.3.4 for details) with the exception of low-mass evolved Helium stars for which there is not much known about magnetic fields. For fully convective MS stars ($K_{\rm i} = 0$, $M < 0.35$ M$_\odot$) magnetic braking may also operate, although it has been hypothesized that the braking is suppressed (Rappaport, Verbunt & Joss 1983; Zangrilli, Tout & Bianchini 1997) in order to provide an explanation of the observed period gap for cataclysmic variables. Therefore we assume that magnetic braking is not operative for fully convective stars, independent of the prescription used. Since massive core helium burning stars, more massive H-rich MS stars, and He-rich MS stars have radiative envelopes, we assume that magnetic braking does not operate in these stars. The prescription for the loss of angular momentum associated with magnetic braking $dJ_{\rm i,mb}/\,dt$ takes several forms. Historically, most studies have adopted the form suggested by Rappaport et al. (1983) where

$$dJ_{\rm i,mb}/\,dt = -5.8\times10^{-22} M_i {R_i}^{\gamma} {\omega_i}^3 \qquad (10)$$

with parameter $\gamma = 2$ in our model calculations. However, studies based on the observations of rapidly rotating stars show that the Skumanich relation ($\dot{J} \propto \omega^3$) is inadequate in this regime and point to a weakening of magnetic braking due to saturation of the dynamo (Andronov, Pinsonneault & Sills 2003). In this case, the angular momentum loss rate takes the form

$$dJ_{\rm i,mb}/\,dt = -8.88\times10^{-22}\sqrt{R_i/M_i}\begin{cases} {\omega_i}^3 & \omega_i \le \omega_{\rm crit} \\ \omega_i \omega_{\rm crit}^2 & \omega_i > \omega_{\rm crit} \end{cases} \qquad (11)$$

where, i denotes the component for which magnetic braking is operating, $\omega_{\rm i}$ [Myr^{-1}] is angular velocity, and $\omega_{\rm crit}$

stands for a critical value of angular velocity above which the angular momentum loss rate enters the saturated regime. If the latter law is used, the saturation is applied only for MS stars and $\omega_{\rm crit}$ is interpolated from Table 1 of Andronov et al. (2003).

In addition, we also include the form of magnetic braking from the results of a study by Ivanova & Taam (2003). In this latter study, an intermediate form of the angular momentum loss rate was derived ($\dot{J} \propto \omega^{1.3}$) based on a two component coronal model as applied to the observational data relating stellar activity to stellar rotation. Specifically, we adopt

$$dJ_{\rm i,mb}/\,dt = -619.2 R_i^{\,4} \begin{cases} (\omega_i/9.45\times10^7)^3 & \omega_i \le \omega_{\rm x} \\ 10^{1.7}(\omega_i/9.45\times10^7)^{1.3} & \omega_i > \omega_{\rm x} \end{cases} \quad (12)$$

with $w_{\rm x} = 9.45 \times 10^8$ Myr^{-1}. This law is used for the `StarTrack` standard model calculations.

3.3. *Tidal Evolution*

The evolution of the orbital parameters (a, e) as well as component spins ($\omega_{\rm i}$, $i = 1, 2$) driven by tidal interactions of binary components is computed in the standard equilibrium-tide, weak- friction approximation (Zahn 1977, 1989), following the formalism of Hut (1981)[1]. This formalism allows us to treat binaries with arbitrarily large eccentricities. We assume that the only sources of dissipation are eddy viscosity in convective envelopes and radiative damping in radiative envelopes. Specifically, we integrate numerically the following differential equations in parallel with the stellar evolution

$$\left(\frac{da}{dt}\right)_{\rm tid} = -6F_{\rm tid}\left(\tfrac{k}{T}\right)_{\rm i} q_{\rm i}(1+q_{\rm i})\left(\tfrac{R_{\rm i}}{a}\right)^8 \tfrac{a}{(1-e^2)^{15/2}} \times \left(f_1(e^2) - (1-e^2)^{3/2} f_2(e^2)\tfrac{\omega_{\rm i}}{\omega_{\rm orb}}\right) \quad (13)$$

$$\left(\frac{de}{dt}\right)_{\rm tid} = -27F_{\rm tid}\left(\tfrac{k}{T}\right)_{\rm i} q_{\rm i}(1+q_{\rm i})\left(\tfrac{R_{\rm i}}{a}\right)^8 \tfrac{e}{(1-e^2)^{13/2}} \times \left(f_3(e^2) - \tfrac{11}{18}(1-e^2)^{3/2} f_4(e^2)\tfrac{\omega_{\rm i}}{\omega_{\rm orb}}\right) \quad (14)$$

$$\left(\frac{d\omega_{\rm i}}{dt}\right)_{\rm tid} = 3F_{\rm tid}\left(\tfrac{k}{T}\right)_{\rm i} \tfrac{q_{\rm i}^2}{r_{\rm i,gyr}^2}\left(\tfrac{R_{\rm i}}{a}\right)^6 \tfrac{\omega_{\rm orb}}{(1-e^2)^6} \times \left(f_2(e^2) - (1-e^2)^{3/2} f_5(e^2)\tfrac{\omega_{\rm i}}{\omega_{\rm orb}}\right) \quad (15)$$

where
$f_1(e^2) = 1 + \frac{31}{2}e^2 + \frac{255}{8}e^4 + \frac{185}{16}e^6 + \frac{25}{64}e^8$
$f_2(e^2) = 1 + \frac{15}{2}e^2 + \frac{45}{8}e^4 + \frac{5}{16}e^6$
$f_3(e^2) = 1 + \frac{15}{4}e^2 + \frac{15}{8}e^4 + \frac{5}{64}e^6$
$f_4(e^2) = 1 + \frac{3}{2}e^2 + \frac{1}{8}e^4$
$f_5(e^2) = 1 + 3e^2 + \frac{3}{8}e^4$
and $r_{\rm i,gyr}$ is the gyration radius and is defined by $I_{\rm i} \equiv M_{\rm i}(r_{\rm i,gyr}R_{\rm i})^2$, with $I_{\rm i}$ denoting the moment of inertia of a given binary component. Here the mass ratio is defined as follows,

$$q_{\rm i} = \begin{cases} M_2/M_1 & i = 1 \\ M_1/M_2 & i = 2 \end{cases} \quad (16)$$

The quantity $(k/T)_{\rm i}$ is the ratio of the apsidal motion constant k (which depends on the interior structure of the star) over the timescale T of tidal dissipation. Following Hurley, Tout & Pols (2002), we calculate that constant for either the equilibrium tide with convective damping ($(k/T)_{\rm i} = (k/T)_{\rm i,con}$) or the dynamical tide with radiative damping ($(k/T)_{\rm i} = (k/T)_{\rm i,rad}$). Radiative damping is applied to stars with radiative envelopes: MS stars with mass over $M_{\rm ms,conv}$, CHeB stars with mass over 7 $M_\odot$, massive evolved He stars and all He MS stars. For all other stars, convective damping is applied (see § 2.3.4 for details on convective/radiative envelopes). We do not calculate tides on stellar remnants, e.g., on WDs ($K_{\rm i} \ge 10$).

The constant for convective damping is obtained from

$$\left(\frac{k}{T}\right)_{\rm i,con} = \frac{2}{21}\frac{f_{\rm i,conv}}{\tau_{\rm i,conv}}\frac{M_{\rm i,env}}{M_{\rm i}}\ {\rm yr}^{-1} \quad (17)$$

where $M_{\rm i,env}$ is the mass contained in the convective envelope of component i. The eddy turnover time $\tau_{\rm i,conv}$ is calculated as

$$\tau_{\rm i,conv} = 0.431\left[\frac{M_{\rm i,env}R_{\rm i,env}(R_{\rm i} - \frac{1}{2}R_{\rm i,env})}{3L_{\rm i}}\right]^{1/3} {\rm yr} \quad (18)$$

with $R_{\rm i,env}$ denoting the depth of the convective envelope and $L_{\rm i}$ the bolometric luminosity of a given component (Rasio et al. 1996).

The numerical factor $f_{\rm i,conv}$ is defined as

$$f_{\rm i,conv} = min\left[1, \left(\frac{P_{\rm i,tid}}{2\tau_{\rm i,conv}}\right)^2\right] \quad (19)$$

with the tidal pumping timescale $P_{\rm i,tid}$ defined as

$$\frac{1}{P_{\rm i,tid}} = \left|\frac{1}{P_{\rm orb}} - \frac{1}{P_{\rm i,spin}}\right| \quad (20)$$

where $P_{\rm orb}$ and $P_{\rm i,spin}$ are the binary orbital period and the spin period of component i, respectively. This factor represents the reduction in the effectiveness of eddy viscosity when the forcing period is less than the turnover period of the largest eddies (Goldreich & Keeley 1977)

The constant for radiative damping is calculated from

$$\left(\frac{k}{T}\right)_{\rm i,rad} = 1.9782\times10^4\frac{M_{\rm i}R_{\rm i}}{a}(1+q_2)^{5/6}E_2\ {\rm yr}^{-1} \quad (21)$$

where a second-order tidal coefficient $E_2 = 1.592 \times 10^{-9}M_{\rm i}^{2.84}$ was fitted (Hurley et al. 2002) to values given by Zahn (1975).

Finally, we have introduced an additional scaling factor $F_{\rm tid}$ in the evolution equations (eq. 13, 14, 15) which we normally set to: $F_{\rm tid} = 10$. This factor makes tidal forces (both in case of convective and radiative damping) more effective than predicted by the standard Zahn theory. The choice of this specific value of $F_{\rm tid}$ is a result of our calibration against the cutoff period for circularization of binaries

[1]Note that upon entering RLOF any binary system is instantly synchronized and circularized.

in M67 and from the orbital decay of the high mass X-ray binary LMC X-4 (for details see § 8.2).

The orbital angular momentum change associated with tides is calculated from

$$dJ_{\rm i,tid}/\,dt = 3F_{\rm tid}I_{\rm i}\left(\frac{k}{T}\right)_{\rm i}\frac{q_{\rm i}^2}{r_{\rm i,gyr}^2}\left(\frac{R_{\rm i}}{a}\right)^6\frac{\omega_{\rm orb}}{(1-e^2)^6} \times\left(f_2(e^2)-(1-e^2)^{3/2}f_5(e^2)\frac{\omega_{\rm i}}{\omega_{\rm orb}}\right) \quad (22)$$

and the orbit shrinks when $dJ_{1,\rm tid}/\,dt + dJ_{2,\rm tid}/\,dt$ is negative and expands otherwise.

Pre–main sequence tidal synchronization and circularization. We also allow for pre-MS tidal interactions. Since we do not follow pre-MS evolution, all binaries with orbital periods shorter than 4.3 d (Mathieu et al. 1992) are simply assumed to have circularized and all binary components to have synchronized by the time they reach the ZAMS. For binaries with longer orbital periods we apply our assumed distribution of initial eccentricities (see § 7) and initial rotational velocities for binary components (see § 2.3.3).

Darwin instability. One important consequence of tidal interactions in massive binaries is the possible occurrence of the Darwin instability (e.g., Lai et al. 1993). When the more massive component is spinning slowly compared to the orbital rate of its companion, tidal forces will tend to spin it up, leading to loss of orbital angular momentum (orbital decay). Usually this orbital decay will stop when synchronization is established. However, if, in the synchronized state, more than a third of the total binary angular momentum would be in the component spins, then synchronization can never be reached and the components will continue to spiral in. We follow this process until one of the binary components overflows its Roche lobe. The ensuing mass transfer may stabilize the orbital decay, and the system is then followed through this stable RLOF phase. In cases where the RLOF is found to be dynamically unstable (§ 5.1 and § 5.2) the system goes through a CE phase leading either to a merger, or further orbital decay with envelope ejection (§ 5.4).

3.4. *Mass and Angular Momentum Loss from Binaries*

Mass lost from the binary components in stellar winds carries angular momentum, in turn affecting the orbit through tidal coupling. Similarly, during RLOF, some of the transferred material and its associated angular momentum may be lost from the system. In this section we consider the amount of angular momentum loss associated both with stellar winds and RLOF phases. However, for RLOF we only consider here dynamically stable phases, while the change of the orbit following unstable RLOF (common envelope events) is described in § 5.4.

For stellar winds we assume spherically symmetric mass loss, which carries away the specific angular momentum of the mass–losing component. The corresponding change of the orbit (Jeans-mode mass loss) is calculated from

$$a(M_1+M_2) \;=\; \text{const.} \quad (23)$$

The above approach holds for circular orbits, however the change in binary separation a is similar for eccentric orbits (Vanbeveren, Van Rensbergen & De Loore 1998).

In case of stable RLOF with compact accretors (WD, NS, BH; $K_{\rm acc} = 10, 11, 12, 13, 14, 16, 17$) we limit (although that assumption may be relaxed) accretion to the Eddington critical rate

$$\dot{M}_{\rm edd} = 2.088\times10^{-3}\frac{R_{\rm acc}}{\epsilon(1+X)}\ {\rm M}_\odot\ {\rm yr}^{-1} \quad (24)$$

and the corresponding critical Eddington luminosity may be expressed as

$$L_{\rm edd} = \epsilon\frac{GM_{\rm acc}\dot{M}_{\rm edd}}{R_{\rm acc}} \quad (25)$$

where $R_{\rm acc}$ denotes the radius at which the accretion onto compact object takes place (a NS or a WD radius, and three Schwarzschild radii for a BH), X denotes the composition of accreted material (0.7 for the H-rich material, and 0.0 for all other compositions), and ϵ gives the conversion efficiency of gravitational binding energy to radiation associated with accretion onto a WD/NS (surface accretion $\epsilon = 1.0$) and onto a BH (disk accretion $\epsilon = 0.5$). We also note that above some critical (very high) accretion rate, nuclear burning will start on the WD surface. This will be much more radiatively efficient than the gravitational energy release and the above relations break down. If the mass transfer rate is higher than $\dot{M}_{\rm edd}$ the excess material leaves the system from the vicinity of the accreting object and thus carries away the specific angular momentum of the accretor. The angular momentum loss associated with a given systemic mass loss in a RLOF phase is obtained from

$$dJ_{\rm RLOF}/\,dt = -R_{\rm com}^2 w_{\rm orb}(1-f_{\rm a})\dot{M}_{\rm don} \quad (26)$$

where $R_{\rm com} = aM_{\rm don}/(M_{\rm don}+M_{\rm acc})$ is the distance between the accretor and binary center of mass, and $\dot{M}_{\rm don}$ is the mass transfer rate (donor RLOF rate, see eq. 44). The $f_{\rm a}$ fraction of material transferred from the donor is accreted on the compact object. If mass transfer is sub-Eddington then $f_{\rm a} = 1$ (conservative), otherwise it is $f_{\rm a} = \dot{M}_{\rm edd}/\dot{M}_{\rm don}$ (non-conservative evolution). Here we assume that the radiative efficiency is not a function of the mass transfer rate. Some work has suggested that at high transfer rates, flows onto black holes may become radiatively inefficient as photons are trapped in the flow and advected into the black hole (see e.g., Abramowicz et al. 1988), or that substantially super-Eddington accretion may be possible in non-spherical accretion flows (e.g., Begelman 2002). In the current version of the code, we do not consider these possibilities.

For all other, non-degenerate donors ($K_{\rm acc} = 0, 1, 2, 3, 4, 5, 6, 7, 8, 9$) we assume a non-conservative evolution through stable RLOF, with part of the mass lost by the donor accreted onto the companion ($f_{\rm a}$), and the rest $(1-f_{\rm a})$ leaving the system with a specific angular momentum expressed in the units of binary angular momentum ($2\pi ja^2/P_{\rm orb}$; see Podsiadlowski, Joss & Hsu 1992). The angular momentum loss is then estimated from

$$dJ_{\rm RLOF}/\,dt = -j_{\rm loss}\frac{J_{\rm orb}}{M_{\rm don}+M_{\rm acc}}(1-f_{\rm a})\dot{M}_{\rm don} \quad (27)$$

where $j_{\rm loss} = 1$ which corresponds to mass loss through the L_1 point. For our standard model calculation we adopt

$f_a = 0.5$ (half of the transferred mass lost from system, e.g. Meurs & van den Heuvel 1989) and $j = 1$ (mass lost with the specific angular momentum of the binary, e.g. Podsiadlowski et al. 1992).

4. WIND MASS LOSS/ACCRETION IMPLEMENTATION

We adopt the compilation of mass loss rates from Hurley at al. (2000). We have further extended the original formulae to include winds from low- and intermediate-mass MS stars. The structure of the star (and its subsequent evolution) in response to stellar wind mass loss is self-consistently taken into account with the Hurley et al. (2000) evolutionary formulae. The most important changes include possible removal of the H-rich envelope of a massive star or a more gradual nuclear evolution with decreasing mass. The effects of wind mass loss from binary components on the orbital parameters are also accounted for (see § 3.4).

The effects of mass increase of binary components due to accretion from the companion winds are neglected. Either the wind accretion rates are very low or the high wind accretion phases do not last for long, which does not translate into significant mass increase of a companion star. However, we estimate the wind accretion rates onto NSs and BHs since it may give rise to bright X-ray emission (see § 9).

The wind accretion rate is calculated in the general case of eccentric orbits, i.e. we obtain accretion rate (and accretion luminosity) for a specified position on the orbit, or we integrate over a specific part of the orbit (e.g., corresponding to the exposure time of given observations). This may be of importance for eccentric wind-fed binaries, e.g., high mass X-ray binaries (see § 9.2). We have also implemented an orbital-averaged solutions. The two solutions may be alternated as required for a given project or analysis.

4.1. *General Eccentric Orbit Case*

We follow the Bondi & Hoyle (1944) accretion model to calculate the accretion from stellar wind. As an approximation we may express (Boffin & Jorissen 1988) the accretion rate as

$$\dot{M}_{\rm acc,wind} = \alpha_{\rm wind} \frac{2\pi (G M_{\rm acc})^2}{(V_{\rm rel}^2 + c_{\rm wind}^2)^{3/2}} \rho \qquad (28)$$

where $\alpha_{\rm wind} = 1.5$ is the accretion efficiency in the Bondi–Hoyle model, although it may be as low as 0.05 in some specific cases (e.g., see hydrodynamical simulations of Theuns, Boffin & Jorissen 1996 for Barium star formation), $c_{\rm wind}$ is the wind sound speed, and $V_{\rm rel}$ is the relative velocity of the wind with respect to the accreting star. The local (undisturbed) density of the wind matter ρ in the vicinity of the accreting object may be calculated in a steady spherically symmetric case from

$$\dot{M}_{\rm don,wind} = -4\pi r^2 \rho V_{\rm wind} \qquad (29)$$

where $\dot{M}_{\rm don,wind}$ is the wind mass loss rate form the donor, r is the instantaneous distance between the two stars, and $V_{\rm wind}$ is the wind velocity. We assume that the wind flow is supersonic ($V_{\rm rel} \gg c_{\rm wind}$) so that $c_{\rm wind}^2$ may be dropped from eq. 28. We introduce ρ (expressed through eq. 29) into eq. 28 to obtain

$$\dot{M}_{\rm acc,wind} = -\alpha_{\rm wind} \frac{(G M_{\rm acc})^2}{2 V_{\rm rel}^3 V_{\rm wind} r^2} \dot{M}_{\rm don,wind} \qquad (30)$$

The accretion rate calculated with eq. 30 varies as the accreting object moves in its orbit around mass–losing star. The relative distance r of the two stars is obtained through the Kepler equation for a given orbit. Obviously r is a function of orbital position. The vector of the relative velocity $\vec{V}_{\rm rel}$ is defined as

$$\vec{V}_{\rm rel} = \vec{V}_{\rm acc,orb} + \vec{V}_{wind} \qquad (31)$$

where $\vec{V}_{\rm acc,orb}$ denotes the instantaneous velocity of the accretor on the orbit relative to the mass loosing star, and is readily obtained for a given position through the Kepler equation. The direction of the wind velocity vector $\vec{V}_{wind}$ follows the vector pointing toward the accretor on its relative orbit around the mass–losing star. We set the wind velocity proportional to the escape velocity from the surface of the mass–losing star

$$V_{\rm wind}^2 = 2\beta_{\rm wind} \frac{G M_{\rm don}}{R_{\rm don}}, \qquad (32)$$

and vary $\beta_{\rm wind}$ with the spectral type of the mass–losing star (Hurley et al. 2002). For extended ($R_{\rm don} > 900$ R$_\odot$) H-rich giants ($K_{\rm don} = 2, 3, 4, 5, 6$) slow winds are assumed $\beta_{\rm wind} = 0.125$. For the most massive MS stars (> 120 M$_\odot$) $\beta_{\rm wind} = 7$, for low mass MS stars (< 1.4 M$_\odot$) $\beta_{\rm wind} = 0.5$ and the value of $\beta_{\rm wind}$ is interpolated in-between. For He-rich stars ($K_{\rm don} = 7, 8, 9$); $\beta_{\rm wind} = 7$ for $M_{\rm don} > 120$ M$_\odot$, $\beta_{\rm wind} = 0.125$ for $M_{\rm don} < 10$ M$_\odot$, and is interpolated in-between.

4.2. *Orbit-averaged Case*

We use eq. 30 to obtain the orbit-averaged accretion rate. The wind velocity vector is assumed to be perpendicular to the orbital speed vector (as on a circular orbit), i.e., $V_{\rm rel}^2 = V_{\rm acc,orb}^2 + V_{wind}^2$. The wind velocity is taken from eq. 32. The orbital velocity of the accretor is taken to be constant and is obtained from the circular orbit approximation $V_{\rm acc,orb}^2 = G(M_{\rm acc} + M_{\rm don})/a$. Finally, $1/r^2$ is substituted in eq. 30 with its mean value over one orbital revolution, i.e., $1/(a^2\sqrt{1-e^2})$ to obtain

$$\dot{M}_{\rm acc,wind} = -\frac{F_{\rm wind}}{\sqrt{1-e^2}} \left(\frac{G M_{\rm acc}}{V_{\rm wind}^2} \right)^2 \frac{\alpha_{\rm wind}}{2a^2} \frac{\dot{M}_{\rm don,wind}}{(1+V^2)^{3/2}} \qquad (33)$$

where $F_{\rm wind}$ is a parameter (see below) and $V^2 = V_{\rm acc,orb}^2 / V_{\rm wind}^2$.

For highly eccentric orbits, the averaged (over one orbit) accretion rate calculated with the eq. 33 may exceed the companion mass loss rate. This is a direct result of the orbital averaging used above. To avoid this we follow Hurley et al. (2002; § 2.1) and adopt $F_{\rm wind}$ such that $\dot{M}_{\rm acc,wind}$ never exceeds $0.8\dot{M}_{\rm don,wind}$.

5. ROCHE LOBE OVERFLOW CALCULATIONS

Different physical processes may be responsible for driving RLOF. In the following we describe the treatment of mass loss and mass accretion in our model.

5.1. *Mass Transfer/Accretion Rate*

For any binary system during RLOF phases with a non-degenerate donor ($K_{\rm don} < 10$) we calculate the radius mass exponents for the donor and its Roche lobe

$$\zeta_{\rm don} = \frac{\partial \ln R_{\rm don}}{\partial \ln M_{\rm don}} \tag{34}$$

$$\zeta_{\rm lob} = \frac{\partial \ln R_{\rm don,lob}}{\partial \ln M_{\rm don}} \tag{35}$$

and we estimate the change of donor radius with time due to its nuclear evolution as

$$\zeta_{\rm evl} = \frac{\partial \ln R_{\rm don}}{\partial t} \tag{36}$$

RLOF may be driven by different physical processes; angular momentum losses connected to magnetic braking and gravitational radiation or expansion due to nuclear evolution. The timescales for magnetic braking, tides, and gravitational radiation are calculated from

$$\tau_{\rm mb} = -\frac{J_{\rm orb}}{dJ_{\rm don,mb}/\,dt + dJ_{\rm acc,mb}/\,dt} \tag{37}$$

$$\tau_{\rm tid} = -\frac{J_{\rm orb}}{dJ_{\rm don,tid}/\,dt + dJ_{\rm acc,tid}/\,dt} \tag{38}$$

$$\tau_{\rm gr} = -\frac{J_{\rm orb}}{dJ_{\rm gr}/\,dt} \tag{39}$$

where expressions for $dJ_{\rm gr}/\,dt$, $dJ_{\rm i,mb}/\,dt$, $dJ_{\rm i,tid}/\,dt$ are given in § 3.1, § 3.2 and § 3.3, respectively.

If RLOF is driven by the combination of angular momentum losses changing the orbit and nuclear evolution of the donor we then calculate the mass transfer rate from

$$\dot{M}_{\rm eq} = -\frac{\zeta_{\rm evl} + \frac{2}{\tau_{\rm mb}} + \frac{2}{\tau_{\rm tid}} + \frac{2}{\tau_{\rm gr}}}{\zeta_{\rm don} - \zeta_{\rm lob}} M_{\rm don} \tag{40}$$

and the corresponding mass transfer timescale

$$\tau_{\rm eq} = -\frac{M_{\rm don}}{\dot{M}_{\rm eq}} \tag{41}$$

Additionally we estimate the thermal timescale for the donor following Kalogera & Webbink (1996) from

$$\tau_{\rm th} = \frac{30 \times {M_{\rm don}}^2}{R_{\rm don} L_{\rm don}} \tag{42}$$

and the mass transfer rate on the thermal timescale

$$\dot{M}_{\rm th} = -\frac{M_{\rm don}}{\tau_{\rm th}} \tag{43}$$

In the case of stable RLOF, $\tau_{\rm eq} > \tau_{\rm th}$, we use eq. 40 to calculate the mass transfer rate. Otherwise, for $\tau_{\rm eq} \leq \tau_{\rm th}$, RLOF becomes unstable on the thermal timescale and we evolve a given system calculating the mass transfer rate from eq. 43). However, in some cases the RLOF is so rapid that it may eventually lead to a dynamical instability. Once the $\dot{M}_{\rm eq}$ changes sign and becomes positive, we get the indication that the RLOF evolves on very fast timescale, the donor loses its equilibrium, and the system evolves either on the thermal or dynamical timescale. In this case a special *diagnostic diagram* is used (see below) to decide which of the two timescales is relevant. We also allow for the development of a delayed dynamical instability, which may occur for stars with radiative envelope, but with a deep convective layer. Dynamical instability during RLOF leads to spiral-in of binary components and a common envelope evolution (CE). We follow the CE phase to determine whether the binary survives (ejection of the envelope at the expense of orbital energy) or if a merger of the binary components (single star formation) occurs.

The following summarizes the calculation of the RLOF mass transfer rates

$$\dot{M}_{\rm don} = \begin{cases} CE/merger & M_{\rm don} > q_{\rm ddi} \times M_{\rm acc} \\ \dot{M}_{\rm eq} & \dot{M}_{\rm eq} < 0 \; and \; \tau_{\rm eq} > \tau_{\rm th} \\ \dot{M}_{\rm th} & \dot{M}_{\rm eq} < 0 \; and \; \tau_{\rm eq} <= \tau_{\rm th} \\ \dot{M}_{\rm th}/CE/merger & diagnostic \; diagram \end{cases} \tag{44}$$

where we additionally assume that above some critical mass ratio ($q_{\rm ddi} \equiv M_{\rm don}/M_{\rm acc}$) the binary system will evolve toward delayed dynamical instability (Hjellming & Webbink 1987), leading to rapid inspiral and CE evolution. For H-rich stars Hjellming (1989) gives a range $q_{\rm ddi} = 2-4$ depending on the evolutionary state of a donor, while Ivanova & Taam (2004) obtain $q_{\rm ddi} = 2.9 - 3.1$. In our standard model calculations we adopt $q_{\rm ddi} = 3$ for H-rich stars ($K_{\rm i} = 0, 1, 2, 3, 4, 5, 6$). For He-rich stars we adopt critical mass ratios from Ivanova et al. (2003); $q_{\rm ddi} = 1.7$ for HeMS stars ($K_{\rm i} = 7$), while $q_{\rm ddi} = 3.5$ for evolved He stars ($K_{\rm i} = 8, 9$). Also, dynamical instability may be encountered if the trapping radius of the accretion flow exceeds the Roche lobe radius of the accretor (§ 5.4). Additionally, we consider the case of spiral–in in the case of Darwin instability, where the components spin angular momentum is comparable to the orbital angular momentum (§ 3.3).

For the donor stars without a well defined core-envelope structure ($K_{\rm don} = 0, 1, 7, 10, 11, 12, 16, 17$) we assume that the dynamical instability during RLOF *always* leads to a merger. The same is assumed for the donor in the Hertzsprung gap ($K_{\rm don} = 2$) as there is no clear entropy jump at the core-envelope transition (Ivanova & Taam 2004; Belczynski & Taam 2004a). In the case of a merger a single stellar object is formed. However, we do not follow its evolution here. This may lead to an underestimate of our synthetic supernovae rate, since potentially some merger products are massive enough to evolve and explode as Type II or Ib/c SNe. For H-rich and He-rich giant-like donors ($K_{\rm don} = 3, 4, 5, 6, 8, 9$) we follow CE evolution, and assuming ejection of the entire donor envelope, we calculate the most probable outcome with conservation of energy (see § 5.4). If RLOF is encountered for a system with an evolved Helium star donor ($K_{\rm i} = 8, 9$), then it is found that for low donor masses ($\lesssim 4 - 5$ M$_\odot$) RLOF is stable (although it may proceed at very high rates) while for higher donor masses it leads to a CE phase (e.g., see Ivanova et al. 2003). The survival of the binary then depends on the donor properties (e.g., envelope binding energy, its mass, binary separation).

The mass accretion rate in a dynamically stable RLOF is calculated from

$$\dot{M}_{\rm acc} = f_{\rm a} \dot{M}_{\rm don} \tag{45}$$

where $\dot{M}_{\rm don}$ is the donor RLOF mass transfer rate (see eq. 44). The parameter $f_{\rm a}$ denotes the fraction of the transferred mass which is accreted, while the rest $(1 - f_{\rm a})$ is ejected from the system (see § 3.4). Mass accretion in dynamically unstable cases (CE events) is calculated only for NS and BH accretors, since only then significant accretor mass gain may be expected despite very short timescales (for details see BKB02).

5.2. *Diagnostic Diagram for Rapid Mass Transfer*

The aforementioned diagnostic diagram is shown in Fig 2. Once RLOF becomes unstable we do not have proper stellar models to use and calculate the donor properties (e.g., RLOF rate). Therefore, we use an approximate method and calibrate it based on the results from detailed stellar evolutionary and mass transfer calculations, which are not limited to stars in thermal equilibrium. When the donor loses its equilibrium, we use the stellar and binary properties to predict whether the system will evolve through the phase of thermal mass transfer and the donor will regain its equilibrium, or the RLOF will become dynamically unstable and will eventually lead to CE evolution. We plot the donor Roche lobe radius versus decreasing donor mass under the assumption that mass transfer is non-conservative and proceeds on a thermal timescale (see eqs. 42 and 43). For NS/BH accretors the accretion rate is limited by the Eddington rate, while for all other accretors, a fraction $f_{\rm a}$ of transferred material is accreted. The associated specific angular momentum loss is described in § 3.4. As the mass of the donor decreases with mass transfer the Roche lobe first shrinks and then at some critical mass ratio ($q_{\rm low}$), it starts to expand again (see the solid line on the top panel, Fig. 2). If the mass ratio at the moment the star loses its equilibrium $q_{\rm int}$ is not greatly different than $q_{\rm low}$ we expect that the donor may regain the equilibrium when the system is expanding. The dashed line arrow in Figure 2 shows the expected behavior of the donor when it loses its equilibrium. If the system does not evolve into a CE phase then we expect the donor to regain its equilibrium at the position indicated by the arrow. Of course this is just an approximation, since, as the donor evolves, the radius-mass exponent changes. We use a number of published (Tauris & Savonije 1999; Wellstein & Langer 1999; Wellstein, Langer & Braun 2001; Dewi & Pols 2003) and unpublished (N. Ivanova 2004, private communication) detailed calculations to calibrate the diagnostic diagram. Based on these studies we find that a CE phase ensues if

$$CE \begin{cases} q_{\rm int} \geq 1.2\ q_{\rm low} & K_{\rm don} = 2,3,4,5,6 \\ q_{\rm int} \geq 2.0\ q_{\rm low} & K_{\rm don} = 0,1,7,8,9 \end{cases} \tag{46}$$

Otherwise the system is evolved through RLOF on a thermal timescale.

5.3. *Thermal Timescale Mass Transfer*

Once a binary is identified as a thermal timescale RLOF system, we assume that the mass transfer rate remains constant throughout the entire episode. We calculate the rate using eq. 43 where we use properties corresponding to the time the donor loses its thermal equilibrium. This may be justified by the following: *(i)* thermal mass transfer rates have been shown to be rather constant within a factor of $\sim 2-3$ (Paczynski 1971), *(ii)* since the rates are calculated at the time the star loses equilibrium, it is a good approximation (and the best possible with only equilibrium stellar models being available) for the short lived phase of thermal mass transfer that follows.

In the bottom panel of Figure 2 we show an example calculation through a thermal RLOF phase, followed with a slower (driven by nuclear evolution) RLOF period after the donor has regained its thermal equilibrium. The specific system was chosen to match the RLOF calculation of Wellstein et al. (2001) for a 16 $M_\odot$ and 15 $M_\odot$ binary with an initial period of 8 days. The RLOF starts when the primary evolves off the main sequence and crosses the Hertzsprung Gap. Mass transfer initially proceeds on a thermal timescale at a very high rate ($\sim 2.8 \times 10^{-3}$ $M_\odot$ yr^{-1}), then the star regains its equilibrium and the RLOF rate decreases with time by more than order of magnitude ($\sim 10^{-4}$ $M_\odot$ yr^{-1}). Our calculation can be directly compared to Wellstein et al. (2001): see their Figure 4, left panel. Their detailed stellar evolution calculation shows a thermal RLOF rate of $\sim 10^{-3}$ $M_\odot$ yr^{-1}, followed by a slower RLOF phase characterized by rates of $\sim 10^{-4}$ $M_\odot$ yr^{-1}, very similar to what we find with our simplified prescription. Our RLOF phase lasts about twice as long as that of Wellstein et al. (2001), who in contrast to our calculation assumed conservative evolution and did not include effects of tidal spin-orbit interactions. We choose not to modify our standard model assumptions (e.g., neglect tidal interactions) for comparisons, and therefore emphasize some differences with previous calculations. More comparisons of RLOF sequences are presented in § 8.1.

5.4. *Dynamical Instability and Common Envelopes*

Dynamically unstable mass transfer may be encountered in a number of ways. Most often it is a direct consequence of stellar expansion during nuclear evolution. However, loss of orbital angular momentum (e.g., via magnetic braking, gravitational radiation, or tides) may also lead to dynamical instability.

Additionally, we allow a system to evolve into a CE phase if the trapping radius of the accretion flow exceeds the Roche lobe radius of the accretor. The trapping radius is defined as (Begelman 1979)

$$R_{\rm trap} = \frac{\dot{M}_{\rm don}}{\dot{M}_{\rm edd}} \frac{R_{\rm acc}}{2}. \tag{47}$$

Following King & Begelman (1999) and Ivanova et al. (2003) we check whether the mass transfer rate exceeds a critical value above which the system is engulfed in a CE

$$\dot{M}_{\rm trap} = 2 \times \dot{M}_{\rm edd} \frac{R_{\rm acc,lob}}{R_{\rm acc}} \tag{48}$$

where $R_{\rm acc,lob}$ is the accretor Roche lobe radius, and $\dot{M}_{\rm edd}$ is the Eddington critical accretion rate (see eq. 24).

Below we present two different implementations of the orbital contraction calculation during CE that are incorporated in `StarTrack`.

Standard Energy Balance Prescription If dynamical instability is encountered a binary may enter a CE phase. We use the standard energy equations (Webbink 1984) to calculate the outcome of the CE phase

$$\alpha_{\rm ce}\left(\frac{GM_{\rm don,fin}M_{\rm acc}}{2A_{\rm fin}}-\frac{GM_{\rm don,int}M_{\rm acc}}{2A_{\rm int}}\right)=\frac{GM_{\rm don,int}M_{\rm don,env}}{\lambda R_{\rm don,lob}} \quad (49)$$

where, $M_{\rm don,env}$ is the mass of the donor envelope ejected from the binary, $R_{\rm don,lob}$ is the Roche lobe radius of the donor at the onset of RLOF, and the indices int, fin denote the initial and final values, respectively. The parameter λ describes the central concentration of the donor (de Kool 1990; Dewi & Tauris 2000). The right hand side of equation 49 expresses the binding energy of the donor's envelope, the left hand side represents the difference between the final and initial orbital energy, and $\alpha_{\rm ce}$ is the CE efficiency with which orbital energy is used to unbind the stellar envelope. If the calculated final binary orbit is too small to accommodate the two post-CE binary components then a merger occurs. In our calculations, we combine $\alpha_{\rm ce}$ and λ into one CE parameter, and for our standard model, we assume that $\alpha_{\rm ce}\times\lambda=1.0$. If a compact object spirals in the common envelope it may accrete significant amounts of material because of hyper-critical accretion (Blondin 1986; Chevalier 1989, 1993; Brown 1995). We have incorporated the numerical scheme to include the effects of hyper-critical accretion on NSs and BHs in our standard CE prescription (for details see BKB02).

Alternative Angular Momentum Prescription In addition to the standard prescription for common envelope evolution based on comparing the binding and orbital energies (see above), we investigate the alternative approach proposed by Nelemans & Tout (2005), based on the non-conservative mass transfer analysis by Paczynski & Ziolkowski (1967), with the assumption that the mass loss reduces the angular momentum in a linear way. This leads to reduction of the orbital separation

$$\frac{A_{\rm fin}}{A_{\rm int}}=\left(1-\gamma\frac{M_{\rm don,env}}{M_{\rm tot,int}}\right)\frac{M_{\rm tot,fin}}{M_{\rm tot,int}}\left(\frac{M_{\rm don,int}M_{\rm acc,int}}{M_{\rm don,fin}M_{\rm acc,fin}}\right)^2 \quad (50)$$

where $M_{\rm don,env}$ is the mass of the donor envelope lost by the system, $M_{\rm tot,int}$, $M_{\rm tot,fin}$ are the total masses of the system before and after CE, and γ is a scaling factor. Following Nelemans & Tout (2005) we use $\gamma=1.5$ and note that hyper-critical accretion is not included in this prescription.

The two above prescriptions are extended (e.g., BKB02) to the case in which both stars lose their envelopes, which happens if the stars have giant-like structure ($K_{\rm i}=2,3,4,5,6,8,9$) at the onset of CE phases.

5.5. *Mass Transfer from Degenerate Donors*

Degenerate donors, WDs ($K_{\rm don}=10,11,12,16,17$), are also considered. The RLOF is assumed to be driven by gravitational radiation only

$$\dot{M}_{\rm don}=M_{\rm don}D^{-1}\frac{dJ_{\rm gr}/dt}{J_{\rm orb}} \quad (51)$$

with

$$D=\frac{5}{6}+\frac{1}{2}\zeta_{\rm don}-\frac{1-f_{\rm a}}{3(1+q)}-\frac{(1-f_{\rm a})(1+q)\beta_{\rm mt}+f_{\rm a}}{q} \quad (52)$$

where the mass ratio is defined as $q=M_{\rm acc}/M_{\rm don}$, $f_{\rm a}$ denotes the fraction of transferred material that is accreted by the companion (defined and evaluated in § 3.4), and $\beta_{\rm mt}={M_{\rm acc}M_{\rm don}}^2/(M_{\rm don}+M_{\rm acc})^2$.

5.6. *Effects of Mass Transfer on Stellar Evolution*

Rates of mass loss/gain change the subsequent evolution of stars. We implement RLOF mass loss by adding an extra term in the original Hurley et al. (2000) stellar evolution formulae. We appropriately increase the wind mass loss rate to match the combined effects of wind and RLOF mass loss. In this way we ensure that the subsequent evolution of the donor is correctly followed. To treat mass gain, and accretor rejuvenation, we simply reverse the wind mass loss formulae to add material onto the accreting star. This is carefully calculated: using an appropriate change of variables in the original Hurley et al. (2000) formulae ensures that the accretor is placed on the right evolutionary track (Hurley 2003, private communication).

For simplicity, we assume that the composition of accreted material matches that of the accretor, although this may not always be the case. Only in the case of accretion onto white dwarfs we take into account the composition of accreted material (see § 5.7).

5.7. *Mass Accumulation onto White Dwarfs*

A number of important phenomena, like novae and Type Ia SN explosions or accretion-induced collapses are associated with mass accretion onto WDs. In contrast to previous population synthesis studies, we incorporate the most recent results to estimate the accumulation efficiencies on WDs. In particular we consider accretion of matter of various compositions onto different WD types. We also include the possibility that NS formation can occur via accretion induced collapse (AIC) of a massive ONe white dwarf (e.g., Bailyn & Grindlay 1990; Belczynski & Taam 2004a).

In this section we discuss accumulation of material and growth of WD mass in binary systems. Only during dynamically stable RLOF phases the mass accretion onto WDs may be sustained for a prolonged period of time and hence affect the evolution of accreting WDs. During dynamically unstable cases (i.e., CE evolution) we assume that WDs do not accrete any material. If dynamical instability is encountered for a binary with two white dwarfs we assume that a merger occurs. If the total mass of the two merging WDs is higher than $1.4\,{\rm M}_\odot$ we assume a SN Ia explosion, independent of what type of WDs are merging.

During a phase of sustained mass accumulation the massive ONe WD ($K=12$) may eventually collapse to a NS. We include AIC in our standard model calculations since it naturally follows from the adopted accumulation physics (see below). Since little is known about potential asymmetries of the collapse, we either apply no natal kick (standard model) or a full natal kick (parameter studies)

obtained from Arzoumanian, Chernoff, & Cordes (2002) or Hobbs et al. (2005, see also § 6.2). However, we also allow for the possibility of SN Ia explosion instead of AIC in parameter studies. It is also worth noting the difference between accretion and accumulation. The calculation of accretion rate during stable RLOF was described in § 5.1, and this rate could be used to calculate, for example, the accretion luminosity of the system (mostly in the UV part of spectrum for WD accretors). However, it is believed that in many cases (see below) not all of the accreted material remains on the surface of the accreting WD. Mass is lost either in shell flashes (nova-like explosions) or through optically thick winds blowing from the surface of accreting WDs. To calculate the actual WD mass growth through the RLOF phase we need to know the accumulation efficiency, $\eta_{\rm acu}$, which is defined as

$$\dot{M}_{\rm acu} = \eta_{\rm acu} \dot{M}_{\rm acc} \quad (53)$$

where, $\dot{M}_{\rm acu}$ is the mass accumulation rate on the surface of WD and the mass accretion rate ($\dot{M}_{\rm acc}$) is given by eq. 45. In what follows we discuss the accumulation efficiency in various evolutionary scenarios.

Accretion onto Helium and Hybrid white dwarfs. It is widely accepted that if the mass accretion rate $\dot{M}_{\rm acc}$ from the H-rich donor ($K_{\rm don} = 0, 1, 2, 3, 4, 5, 6, 16$) is smaller than some critical value $\dot{M}_{\rm crit1}$, there are strong nova explosions on the surface of the accreting WD, and no material is accumulated. The accumulation efficiency is $\eta_{\rm acu} = 0.0$, i.e. the entire accreted material is lost from the binary. If $\dot{M}_{\rm acc} > \dot{M}_{\rm crit1}$ then the material piles up on the WD leading to RLOF and eventual inspiral. For giant-like donors we evolve the system through CE to examine if the system survives; for all other donors we call it a merger and halt binary evolution. The critical accretion rate is calculated as

$$\dot{M}_{\rm crit1} = l_0 M_{\rm acc}^{\lambda} (X * Q)^{-1} \ {\rm M}_\odot \ {\rm yr}^{-1} \quad (54)$$

where, $Q = 6 \times 10^{18}$ erg g^{-1} is an energy yield of Hydrogen burning, X is the Hydrogen content of accreted material. For Population I stars (metallicity $Z > 0.01$) we use $X = 0.7, l_0 = 1995262.3, \lambda = 8$, while for Population II stars ($Z \leq 0.01$) we use $X = 0.8, l_0 = 31622.8, \lambda = 5$ (Ritter 1999, see his eq. 10,12 and Table 2).

If the mass accretion rate from the He-rich donor ($K_{\rm don} = 7, 8, 9, 10, 17$) is higher than $\dot{M}_{\rm crit2} = 2 \times 10^{-8}$ M$_\odot$ yr^{-1} all the material is accumulated ($\eta_{\rm acu} = 1.0$) until the accreted layer of material ignites in a helium shell flash. At this point degeneracy is lifted, a main sequence helium star ($K_{\rm acc} = 7$) is formed and further accretion on the helium star is then taken into account. Following the calculations of Saio & Nomoto (1998) we estimate the maximum mass of the accreted shell at which the flash occurs

$$\Delta M = \begin{cases} -7.8 \times 10^4 \dot{M}_{\rm acc} + 0.13 & \dot{M}_{\rm acc} < 1.64 \times 10^{-6} \\ 0 ({\rm instantaneous\ flash}) & \dot{M}_{\rm acc} \geq 1.64 \times 10^{-6} \end{cases} \quad (55)$$

where $\dot{M}_{\rm acc}$ is expressed in M$_\odot$ yr^{-1}.

The newly formed helium star may overfill its Roche lobe, in which case either a single helium star is formed (He or Hyb WD companion, $K_{\rm don} = 10, 17$), a helium contact binary is formed (HeMS companion, $K_{\rm don} = 7$) or the system goes through CE evolution (evolved helium star companion, $K_{\rm don} = 8, 9$).

For accretion rates lower than $\dot{M}_{\rm crit2}$, accumulation is also fully efficient ($\eta_{\rm acu} = 1.0$). However, the SN Ia occurs at a sub-Chandrasekhar mass

$$M_{\rm SNIa} = -400 \dot{M}_{\rm acc} + 1.34 \ {\rm M}_\odot, \quad (56)$$

where $\dot{M}_{\rm acc}$ is expressed in M$_\odot$ yr^{-1}. For mass accretion rates close to $\dot{M}_{\rm crit2}$, the above extrapolations from the results of Hashimoto et al. (1986) yield masses smaller than the current mass of the accretor, and we assume an instantaneous SN Ia explosion. We do not consider the accumulation of heavier elements since they could only originate from more massive WDs (e.g., CO or ONe WDs), which would have smaller radii and could not be donors to lighter He or Hyb WDs.

Accretion onto Carbon/Oxygen white dwarfs. In this case we adopt the prescription from Ivanova & Taam (2004). For H-rich donors and mass accretion rates lower than 10^{-11} M$_\odot$ yr^{-1} there are strong nova explosions and no material is accumulated ($\eta_{\rm acu} = 0.0$). In the range $10^{-11} < \dot{M}_{\rm acc} < 10^{-6}$ M$_\odot$ yr^{-1} we interpolate for $\eta_{\rm acu}$ from Prialnik & Kovetz (1995, see their Table 1). For rates higher than 10^{-6} M$_\odot$ yr^{-1} all accreted material burns into helium ($\eta_{\rm acu} = 1.0$). Additionally we account for the effects of strong optically thick winds (Hachisu, Kato & Nomoto 1999), which blow away any material accreted over the critical rate

$$\dot{M}_{\rm crit3} = 0.7510^{-6} (M_{\rm acc} - 0.4) \ {\rm M}_\odot \ {\rm yr}^{-1}. \quad (57)$$

This corresponds to $\eta_{\rm acu} = \dot{M}_{\rm crit3} / \dot{M}_{\rm acc}$ for $\dot{M}_{\rm acc} \geq \dot{M}_{\rm crit3}$. The accretor is allowed to increase in mass up to 1.4 M$_\odot$, and then explodes as a Chandrasekhar mass SN Ia. In the case of He-rich donors, if the mass accretion rate is higher than $\dot{M}_{\rm crit4}$ helium burning is stable and contributes to the accretor mass ($\eta_{\rm acu} = 1.0$). For rates in the range $\dot{M}_{\rm crit4} \div \dot{M}_{\rm crit5}$ accumulation is calculated from

$$\eta_{\rm acu}^{0.8} = -0.35 (\log \dot{M}_{\rm acc} + 6.1)^2 + 1.02 \ \ [-6.5 \div -6.34]$$

$$\eta_{\rm acu}^{0.9} = -0.35 (\log \dot{M}_{\rm acc} + 5.6)^2 + 1.07 \ \ [-6.88 \div -6.05]$$

$$\eta_{\rm acu}^{1.0} = -0.35 (\log \dot{M}_{\rm acc} + 5.6)^2 + 1.01 \ \ [-6.92 \div -5.93]$$

$$\eta_{\rm acu}^{1.1-1.2} = \begin{cases} 0.54 \log \dot{M}_{\rm acc} + 4.16 \ \ [-7.06 \div -5.95] \\ -0.54 (\log \dot{M}_{\rm acc} + 5.6)^2 + 1.01 \ [-5.95 \div -5.76] \end{cases}$$

$$\eta_{\rm acu}^{1.3} = -0.175 (\log \dot{M}_{\rm acc} + 5.35)^2 + 1.03 \ \ [-7.35 \div -5.83]$$

$$\eta_{\rm acu}^{1.35} = -0.115 (\log \dot{M}_{\rm acc} + 5.7)^2 + 1.01 \ [-7.4 \div -6.05] \quad (58)$$

and represents the amount of material that is left on the surface of the accreting WD of a specific mass (denoted by a superscript on $\eta_{\rm acu}$ in M$_\odot$) after the helium shell flash cycle (Kato & Hachisu 1999, 2004). Logarithms of critical mass accretion rates for a given specific WD mass are given in square brackets: $[\log(\dot{M}_{\rm crit5} / {\rm M}_\odot \ {\rm yr}^{-1}) \div \log(\dot{M}_{\rm crit4} / {\rm M}_\odot \ {\rm yr}^{-1})]$. To obtain the accumulation rate for CO WD within the mass range $0.7 - 1.4$ M$_\odot$ we incorporate results of the closest (by mass) model from the

set of eqs. 58. If the WD mass drops below 0.7 $M_\odot$ we use $\eta_{\rm acu} = 1.0$ and we set $\log \dot{M}_{\rm crit4} = \log \dot{M}_{\rm crit5} = -7.6$ (see Kato & Hachisu 2004). The mass of the CO WD accretor is allowed to increase up to 1.4 $M_\odot$, and then a Chandrasekhar mass SN Ia takes place in the two above He-rich accretion regimes. If mass accretion rates drop below $\dot{M}_{\rm crit5}$, the helium accumulates ($\eta_{\rm acu} = 1.0$) on top of the CO WD and once the accumulated mass reaches 0.1 $M_\odot$ (Kato & Hachisu 1999), a detonation follows and ignites the CO core leading to the disruption of the accretor in a sub-Chandrasekhar mass SN Ia (e.g., Taam 1980; Garcia-Senz, Bravo & Woosley 1999). If the mass of the accreting WD has reached 1.4 $M_\odot$ before the accretion layer has reached 0.1 $M_\odot$ then the accretor explodes in a Chandrasekhar mass SN Ia. Carbon/Oxygen accumulation takes place without mass loss ($\eta_{\rm acu} = 1.0$) and leads to SN Ia if Chandrasekhar mass is reached.

Accretion onto Oxygen/Neon/Magnesium white dwarf. Accumulation onto ONe WDs is treated the same way as for CO WD accretors. The only difference arises when an accretor reaches the Chandrasekhar mass. In the case of ONe WD this leads to an AIC and NS formation, and binary evolution continues (see Belczynski & Taam 2004a, 2004b).

6. SPATIAL VELOCITIES

6.1. *Overview*

All stars (single and binary systems) may be initialized with arbitrary velocities appropriate for a given environment. For example, a galactic rotation curve may be used for a field population of a given galaxy, or a velocity dispersion can be applied for a cluster population. The velocities of stars are then followed throughout their evolution. Single stars and binary systems are subject to recoil (change of spatial velocity) in SN explosions. Additionally, binary systems may be disrupted as a result of an especially violent explosion. We account for both mass/angular momentum losses as well as for SN asymmetries (through natal kicks that NSs and BHs receive at their formation; see below). The detailed description of SN explosion treatment is given in BKB02. Here, we only list the new additions to `StarTrack`. The most important modification allows us to trace velocities of disrupted binary components after a SN explosion. For the first time, a full general approach with explosions taking place on orbits of arbitrary eccentricity (in contrast to circular orbits only) is applied in population synthesis studies (see Belczynski et al. 2005c for first results).

6.2. *Natal Kick Distribution*

At the time of birth, both NSs and BHs receive an additional speed, the so-called natal kick, which is connected to asymmetries in SN explosions. We use the distributions inferred from observed velocities of radio pulsars. We have replaced the natal kick distribution used in BKB02 (Cordes & Chernoff 1998) with two more recent alternatives. One presented by Arzoumanian et al. (2002) is a bimodal distribution with a weighted sum of two Gaussians, one with $\sigma = 90$ km sec^{-1} (40%) and another with $\sigma = 500$ km sec^{-1} (60%). The other was derived by Hobbs et al. (2005) and is a single Maxwellian with $\sigma = 265$ km sec^{-1}. According to this most recent study there is no indication of a bimodal (low- and high-velocity) kick distribution claimed in earlier studies (e.g., Fryer, Burrows & Benz 1998; Cordes & Chernoff 1998; Arzoumanian et al. 2002). If this is indeed true, then some theoretical models built in support of the bimodal kick distribution (e.g., Pfahl et al. 2002b and Podsiadlowski et al. 2004 model of high mass X-ray binaries) may need to be revised. Motions of many hundreds of pulsars are expected to be measured in the next few years. These measurements will provide better constraints on the natal kick distribution (Hobbs et al. 2005). Until then we will use both distributions to assess the associated uncertainties in `StarTrack` calculations.

NSs receive full kicks drawn from one of the above distributions. BH kicks are lowered proportionally to the amount of fallback associated with BH formation

$$V_{\rm bh,kick} = (1 - f_{\rm fb})V \tag{59}$$

where V is the kick magnitude drawn from either Arzoumanian et al. (2002) or Hobbs et al. (2005) distribution, and $f_{\rm fb}$ is a fallback parameter, i.e., the fraction (from 0 to 1) of the stellar envelope that falls back. For the most massive BHs, formed silently (no SN explosion) in a direct collapse ($f_{\rm fb} = 1$) of a massive star to a BH, we assume that no natal kick imparted. Details of the BH kick distribution and BH masses at formation are given in BKB02 (see their § 2.2.5). The adopted natal kick distribution and kick scaling for NSs and BHs can be readily changed for parameter studies (e.g., full BH kicks).

6.3. *Supernova disruptions*

Just prior to the SN explosion, the two components of the binary move with velocities $\vec{v}_1^I$ and $\vec{v}_2^I$, which, in the center of mass (CM) system of coordinates, denoted here with the superscript I, satisfy

$$M_{1,\rm int}\vec{v}_1^I + M_{2,\rm int}\vec{v}_2^I = 0 \tag{60}$$

where M_1 denotes the SN component and M_2 its companion. Subscripts int, fin stand for initial and final values.

We make no assumptions about the orbit; it can have an arbitrary eccentricity, in contrast to the derivation by Tauris & Takens (1998), who assumed that the orbit is circular prior to the explosion. At the moment of a supernova explosion the orbital separation is $r_0\vec{n}$. The exploding star loses its envelope, its mass becomes $M_{1,\rm fin}$ and receives a kick $\vec{w}$, so now its velocity in the coordinate system I is

$$\vec{v}_{1,\rm int}^I = \vec{v}_1^I + \vec{w}\,. \tag{61}$$

The secondary star may be affected by the expanding shell and may receive an additional velocity $\vec{v}_{\rm imp}$, however it has been shown (Kalogera 1996) that the effect of this velocity is small, unless the pre-supernova orbital separation is smaller than $\simeq 3\,R_\odot$. We assume that the velocity of the companion is not affected by the impact of supernova ejecta. We also assume that the velocity of the shell is large and the shell leaves the system quickly, i.e. $v_{\rm shell} >> r_{\rm o}P$, where P is the orbital period of the system prior to the explosion.

In order to calculate the final velocity of the two stars we first transform the velocities to the CM system of the

two post-SN stars. The velocity of this system, denoted as II, in relation to system I is

$$\vec{v}_{\rm CM}^{II} = \frac{M_{1,\rm fin}\vec{v}_{1,\rm int}^{I} + M_2\vec{v}_{2,\rm int}^{I}}{M_{1,\rm fin}+M_2} \tag{62}$$

The relative velocity of the two stars in this system is

$$\vec{v}^{II} = \vec{v}_1^I - \vec{v}_2^I + \vec{w} - \vec{v}_{\rm imp} \tag{63}$$

while the initial direction between the two stars remains the same as in the coordinate system I, $\vec{n}^{II} = \vec{n}^I$. In this new system the relative motion of the stars is a hyperbola in the plane perpendicular to the angular momentum vector:

$$\vec{J} = \mu r_0 \vec{n}^{II} \times \vec{v}^{II}\,, \tag{64}$$

where $\mu = M_{1,\rm fin}M_2/(M_{1,\rm fin}+M_2)$ is the reduced mass of the system. It is convenient now to introduce a third coordinate system III in which the angular momentum $\vec{J}$ lies along the z-axis. The transformation from II to III is a rotation $\mathcal{R}$: $v^{III} = \mathcal{R}v^{II}$,$n^{III} = \mathcal{R}n^{II}$. The orbit in III is described by

$$r = \frac{p}{1+\epsilon\cos\phi} \tag{65}$$

where

$$p = \frac{J^2}{\alpha\mu} \;\;\text{and}\;\; \epsilon = \sqrt{1+\frac{2EJ^2}{\alpha^2\mu}}, \tag{66}$$

with $E = \mu(v^{II})^2/2 - \alpha/|r_0|$ is the (positive) energy of the system, and $\alpha = GM_{1,\rm fin}M_2$. The final velocity, at $r\to\infty$, follows from energy conservation:

$$|\vec{v}_{\rm fin}^{III}| = \sqrt{\frac{2E}{\mu}}. \tag{67}$$

In order to find the direction of the final velocity we note that conservation of angular momentum implies that at infinity ($r\to\infty$): the final relative $\vec{v}_{\rm fin}^{III}$ is parallel to the direction between the stars $\vec{n}_{fin}^{III}$. The initial position of the two stars on the trajectory described by eq. 65 is

$$\cos\varphi_{\rm int} = \frac{1}{\epsilon}\left(\frac{p}{r_0}-1\right). \tag{68}$$

The sign of the angle $\varphi_{\rm int}$ is negative if the two stars initially lie on the descending branch of the hyperbola $\vec{v}_{\rm int}^{III}\vec{r}_0^{II} > 0$ and positive if they are on the ascending one $\vec{v}_{\rm int}^{III}\vec{r}_0^{II} < 0$. In the first case, when the two stars are initially on the descending branch, we need to compare the distance of closest approach on the orbit $r_{\rm min} = p/(1+\epsilon)$ with the radius of the companion star to examine whether the two stars collide instead of escaping to infinity.

We obtain the final position on the trajectory from

$$\cos\varphi_{\rm fin} = -\frac{1}{\epsilon} \tag{69}$$

and $\varphi_{\rm fin} > 0$. Thus the final direction between the two stars at $r=\infty$ is $\vec{n}_{\rm fin}^{III} = T(\varphi_{\rm fin}-\varphi_{\rm int})\vec{n}^{III}$, where $T(\phi)$ is the matrix of rotation around the z-axis, and their relative velocity is:

$$\vec{v}_{\rm fin}^{III} = \sqrt{\frac{2E}{\mu}}\vec{n}_{\rm fin}^{III}. \tag{70}$$

We now have to transform quantities from system III back to system I to obtain the final velocities of the two disrupted binary components in the initial (pre-SN) CM system:

$$v_{1,\rm fin}^I = \mathcal{R}^{-1}\left(\frac{-M_2 v_{\rm fin}^{III}}{M_{1,\rm fin}+M2}\right) + v_{\rm CM}^{II} \tag{71}$$

$$v_{2,\rm fin}^I = \mathcal{R}^{-1}\left(\frac{M_{1,\rm fin} v_{\rm fin}^{III}}{M_{1,\rm fin}+M2}\right) + v_{\rm CM}^{II}. \tag{72}$$

7. DISTRIBUTIONS OF INITIAL PARAMETERS

Each binary system is initiated by four parameters, which are assumed to be independent: the primary mass M_1 (the initially more massive component), the mass ratio $q = M_2/M_1$, where M_2 is the mass of the secondary, the semi-major axis a of the orbit, and the orbital eccentricity e.

For both single stars and binary system primaries, we use the initial mass function adopted from Kroupa, Tout & Gilmore (1993) and Kroupa & Weidner (2003),

$$\Psi(M_1) \propto \begin{cases} {M_1}^{-1.3} & 0.08 \le M_1 < 0.5\ {\rm M}_\odot \\ {M_1}^{-2.2} & 0.5 \le M_1 < 1.0\ {\rm M}_\odot \\ {M_1}^{-\alpha_{\rm imf}} & 1.0 \le M_1 < 150\ {\rm M}_\odot \end{cases} \tag{73}$$

where parameter $\alpha_{\rm imf} = 2.35 - 3.2$, with our standard choice being 2.7 for field populations and 2.35 for cluster populations. Stars are generated within an initial mass range: $M_{\rm min} - M_{\rm max}$, and the range is chosen accordingly based on the targeted stellar population. For example, NS studies would require evolution of single stars within range $\sim 8-25$ M$_\odot$ while the formation of WDs would require an initial range $\sim 0.08-8$ M$_\odot$. Binary evolution, due to mass transfer events (both mass accretion and mass loss) may significantly broaden any of the ranges mentioned above.

Following Kuiper (1935), we assume a flat mass ratio distribution,

$$\Phi(q) = 1 \tag{74}$$

in the range $q = 0-1$. Given the value of the primary mass and the mass ratio, we obtain the mass of the secondary $M_2 = qM_1$.

The distribution of initial binary separations is assumed to be flat in the logarithm (Abt 1983),

$$\Gamma(a) \propto \frac{1}{a}, \tag{75}$$

where a ranges from a minimum value, such that the primary fills at most 50% of its Roche lobe at ZAMS, up to 10^5 R$_\odot$.

Finally, we adopt the thermal-equilibrium eccentricity distribution for initial binaries,

$$\Xi(e) = 2e, \tag{76}$$

in the range $e = 0-1$ (e.g., Heggie 1975; Duquennoy & Mayor 1991).

8. CALIBRATIONS AND COMPARISONS

8.1. *Mass Transfer Sequences*

In the following subsections we present `StarTrack` mass transfer calculations and compare them to published and unpublished results based on the use of stellar evolution and mass transfer codes.

8.1.1. *Case B Mass Transfer: MS+HG binary*

We choose this RLOF sequence from Wellstein et al. (2001, their Case B). We start with a 16 $M_\odot$ + 15 $M_\odot$ ZAMS binary in a 8 day circular orbit. RLOF starts after the primary evolves off the MS. The system at the onset of RLOF (t = 11.7 Myr since ZAMS) is characterized by: $K_1 = 2$, $K_2 = 1$, $P_{\rm orb} = 7^d.9$, $e = 0, M_1 = 15.6\ M_\odot$, $M_2 = 14.7\ M_\odot$, $R_1 = 20.0\ R_\odot$, and $R_2 = 11.8\ R_\odot$. The evolution of the system during the RLOF phase is shown in Figure 4.

The RLOF proceeds on the thermal timescale of the donor, which is rapidly expanding while crossing the Hertzsprung Gap. First, there is a phase characterized by very high mass transfer rates ($\sim 3 \times 10^{-3}\ M_\odot\ {\rm yr}^{-1}$), until the mass ratio is reversed and the donor becomes the less massive binary component. Shortly thereafter, the transfer rate slowly decreases ($\sim 10^{-3} - 10^{-4}\ M_\odot\ {\rm yr}^{-1}$). After the mass ratio reversal the orbit starts expanding instead of contracting in response to mass transfer. Part (50%) of the transferred material is accreted by the companion and the rest is lost from the binary (non-conservative evolution). RLOF terminates when the envelope of the donor is nearly exhausted and its radius contracts below the Roche lobe radius, thereby, causing the system to become detached. The primary loses most of its mass ($M_1 = 4.03\ M_\odot$), while the secondary is rejuvenated ($M_2 = 20.47\ M_\odot$). The orbital period increases to reach ~ 80 days at the end of the RLOF phase.

The calculation of Wellstein et al. (2001) shows similar behavior during this RLOF phase in terms of the duration, mass transfer rate, and orbital period. Final donor masses in both simulations are almost the same, while our accretor mass is significantly smaller than that of Wellstein et al. (2001). This difference stems from their assumption of conservative (no mass loss from binary) binary evolution. Further differences are associated with the fact that Wellstein et al. (2001) did not allow for rejuvenation of the secondary (accretor). That is, the secondary is still on the MS when the primary (former donor) ends its life in a SN explosion. A second RLOF phase ensues after the secondary evolves off the MS and becomes a HG star. Despite the very high mass ratio of 26.5/2.8, Wellstein et al. (2001) find the mass transfer to be dynamically stable. The system evolves to final disruption as the secondary undergoes a SN explosion. In contrast to the above findings, we allow the secondary to be rejuvenated in the first RLOF episode. As it evolves off the MS and overfills its Roche lobe, the second RLOF episode occurs when the secondary (now a donor) is a 20.3 $M_\odot$ HG star and the primary is a 3.8 $M_\odot$ HeMS. This phase directly leads to CE evolution and to a subsequent component merger.

8.1.2. *Case A Mass Transfer: MS+MS binary*

This RLOF sequence is selected from Wellstein et al. (2001, their Case A). We start with a 12 $M_\odot$ + 7.5 $M_\odot$ ZAMS binary in a 2.5 day circular orbit. RLOF starts while the primary still evolves through the MS phase. The system at the onset of RLOF (t = 14.8 Myr since ZAMS) is characterized by: $K_1 = 1$, $K_2 = 1$, $P_{\rm orb} = 2^d.3$, $e = 0, M_1 = 11.9\ M_\odot$, $M_2 = 7.5\ M_\odot$, $R_1 = 8.3\ R_\odot$, and $R_2 = 4.0\ R_\odot$. The evolution of the system during the RLOF phase is shown in Figure 5.

First phase. At first, the RLOF proceeds on the thermal timescale with a mass transfer rate of $\sim 5{\times}10^{-4}\ M_\odot\ {\rm yr}^{-1}$, through the so called rapid case A transfer phase. The transfer rate then rapidly decreases by more than 2 orders of magnitude until the component masses are nearly equal. Subsequent evolution proceeds on the much slower nuclear timescale of the donor with transfer rates below $10^{-6}\ M_\odot\ {\rm yr}^{-1}$. RLOF continues until the final stages of the donor MS lifetime, when the primary contracts and detaches from its Roche lobe. The evolution of the orbital period is characterized by an initial small decrease and then (after the thermal timescale phase has ended) a slow but rather constant increase up to 3.5 days. At that point the primary mass is $\sim 6\ M_\odot$ and the secondary mass $\sim 10\ M_\odot$.

Second phase. After $\sim$ 0.5 Myr the primary starts expanding as it enters the Hertzsprung Gap and RLOF restarts. This mass transfer phase is much more rapid and is driven by expansion of the primary. This phase is characterized by high mass transfer rate ($10^{-4} - 10^{-5}\ M_\odot\ {\rm yr}^{-1}$) and the envelope of the primary is soon (0.2 Myr) exhausted, ending the second RLOF phase. During this relatively short phase, the orbit expands significantly (final orbital period $\sim$ 165 days), while the primary loses most of its mass ($M_1 = 1.1\ M_\odot$) while the secondary, that is still on its MS, is rejuvenated to a much higher mass ($M_2 = 12.8\ M_\odot$). The dramatic orbit expansion is an effect of the rather extreme mass ratio for this system at the time of the second RLOF.

For both RLOF phases non-conservative evolution was applied. The evolution of this system ends when the primary forms a low-mass helium star and the secondary then evolves off MS, initiating a CE phase while crossing the Hertzsprung Gap. This phase leads to inspiral and component merger.

The calculation of Wellstein et al. (2001) shows a qualitatively similar system behavior during both RLOF phases; initial high mass transfer phase, then a slower one, short break in RLOF followed by another rapid phase while the donor evolves off the MS. There are some differences in the final mass of accretor and orbital period which are easily understood in the context of the different treatment of mass loss from the binary system (non-conservative here versus conservative in Wellstein et al. (2001) models). Also as mentioned in § 8.1.1 Wellstein et al. (2001) do not allow for rejuvenation of the accretor star which leads to a different final fate of the system. However, they remark that had rejuvenation been included the system would have ended in a CE merger during the expansion phase of the secondary after MS evolution in agreement with our findings.

8.1.3. *BH-MS binary*

This calculation starts with a 10 $M_\odot$ BH + 5 $M_\odot$ ZAMS star. We let the secondary evolve through about half of

its MS lifetime before bringing the system into contact at $t = 51.3$ Myr (counted from the secondary ZAMS) . The system at the onset of RLOF is characterized by: $K_1 = 14$, $K_2 = 1$, $P_{\rm orb} = 1^d.0$, $e = 0$, $M_1 = 10\ {\rm M}_\odot$, $M_2 = 5\ {\rm M}_\odot$, $R_1 = 0.000042\ {\rm R}_\odot$, and $R_2 = 3.5\ {\rm R}_\odot$. The evolution of the system during the RLOF phase is shown in Figure 6.

First phase. RLOF is stable and proceeds on the nuclear timescale of the secondary with a mass transfer rate of $\sim 2 \times 10^{-8}\ {\rm M}_\odot\ {\rm yr}^{-1}$. Since this rate is sub-Eddington we allow all the transferred material to be accreted onto the primary BH, which increases its mass to $\sim 11.5\ {\rm M}_\odot$, while the secondary mass decreases to $\sim 3.5\ {\rm M}_\odot$. During this phase, the period increases from 1 to 2 days. The phase ends when the secondary begins contraction at the end of its MS life.

Second phase. RLOF restarts when the secondary crosses the Hertzsprung Gap with mass transfer proceeding at the high rate ($\sim 10^{-6}\ {\rm M}_\odot\ {\rm yr}^{-1}$) corresponding to rapid expansion of the star on its thermal timescale during that phase. At some point the donor starts ascending along the red giant branch, and the transfer rate drops by about an order of magnitude to $\sim 3 \times 10^{-7}\ {\rm M}_\odot\ {\rm yr}^{-1}$. Since the transfer rate is super-Eddington throughout this entire phase we limit accretion onto the BH to the Eddington rate, allowing the rest of the material to leave the binary with the specific orbital angular momentum of the BH. In the end the BH has increased its mass to 12.6 $\rm M_\odot$ and the mass of the donor has decreased to 0.6 $\rm M_\odot$. The orbit expands significantly (~ 300 days) during this rapid RLOF phase.

The RLOF phase ends at the point when the donor, due to the loss of its almost entire H-rich envelope, stops its expansion. The system ends its life as a wide BH-WD binary.

The same RLOF sequence was calculated with the detailed stellar evolution code of Ivanova et al. (2003; also see Ivanova & Taam 2004). The comparison of the two phases of RLOF shows overall qualitative agreement with the `StarTrack` calculation. The mass transfer rates are virtually the same: $\sim 2 \times 10^{-8}$ and $\sim 10^{-6}\ {\rm M}_\odot\ {\rm yr}^{-1}$, for first and second phase, respectively. However, the detailed calculation with the evolution code shows a longer duration (by a factor ~ 2) for the first RLOF phase.

8.1.4. *BH-RG binary*

This calculation starts with a 7 $\rm M_\odot$ BH + 2 $\rm M_\odot$ ZAMS star. We let the secondary evolve through about one third of its red giant lifetime before bringing the system into contact at $t = 1180.4$ Myr (counted from the secondary ZAMS). The system at the onset of RLOF is characterized by: $K_1 = 14$, $K_2 = 3$, $P_{\rm orb} = 4^d.8$, $e = 0$, $M_1 = 7\ {\rm M}_\odot$, $M_2 = 2\ {\rm M}_\odot$, $R_1 = 0.000030\ {\rm R}_\odot$, and $R_2 = 7.1\ {\rm R}_\odot$. The evolution of the system during RLOF phase is shown in Figure 7.

RLOF is stable and proceeds through the entire RG phase ($K_2 = 3$) on the nuclear timescale of the donor. The mass transfer rate is sub-Eddington and thus the material transferred to the BH is entirely accreted. In the end the mass of the BH is increased to 8.4 $\rm M_\odot$ while the mass of the donor is decreased to 0.6 $\rm M_\odot$. As the donor expands, ascending the RG branch, the orbit expands as well, and finally the RLOF phase terminates at an orbital period of ~ 90 days. The phase ends when the donor contracts upon igniting helium in its core. The system eventually forms a wide BH-WD binary.

This RLOF sequence was also calculated with the detailed stellar evolution code of Ivanova et al. (2003). The mass transfer rates found in both cases are similar ($\sim 10^{-7} - 10^{-8}\ {\rm M}_\odot\ {\rm yr}^{-1}$) and in this case the `StarTrack` timescales are shorter, but do not differ by more than 50%.

8.1.5. *Short period NS-RG binary*

This RLOF sequence is chosen from Tauris & Savonije (1999, their example 2b). We start with a 1.3 $\rm M_\odot$ NS + 1.6 $\rm M_\odot$ ZAMS star in a 3 day circular orbit. RLOF starts while the secondary is on the RG branch ($t = 2321.4$ Myr since secondary ZAMS) and the binary is described by: $K_1 = 13$, $K_2 = 3$, $P_{\rm orb} = 2^d.8$, $e = 0$, $M_1 = 1.3\ {\rm M}_\odot$, $M_2 = 1.6\ {\rm M}_\odot$, $R_1 = 0.000014\ {\rm R}_\odot$, and $R_2 = 4.7\ {\rm R}_\odot$. The evolution of the system during the RLOF phase is shown in Figure 8.

At first the RLOF proceeds on a thermal timescale with a highly super-Eddington mass transfer rate ($\sim 10^{-6}\ {\rm M}_\odot\ {\rm yr}^{-1}$). After the donor becomes less massive than its accretor, the mass transfer is driven by the expansion of the red giant donor (on its nuclear timescale) at a much smaller rate of $\sim 10^{-8}\ {\rm M}_\odot\ {\rm yr}^{-1}$. As the mass transfer rate decreases, the NS starts to accrete efficiently and its mass increases to 1.9 $\rm M_\odot$. Eventually, after ~ 65 Myr of RLOF, the RG secondary loses most of its mass (0.28 $\rm M_\odot$) and contracts, leaving a remnant helium WD. At this point the RLOF phase ends (orbital period 60 days), and further evolution leads to the formation of wide binary, with a recycled pulsar.

Comparison with the detailed evolutionary calculation of Tauris & Savonije (1999) shows good agreement between the results. The detailed calculations show an initial rapid RLOF phase followed by a sub-Eddington mass transfer phase, eventually leading to the formation of NS-He WD binary. Final component masses (NS and donor: 2.05 and 0.29 $\rm M_\odot$, respectively) are very similar to the ones obtained with `StarTrack`. The final orbital period of 42 days obtained by Tauris & Savonije (1999) is shorter than in our calculation (60 days). In addition, there is a difference in the duration of RLOF phase, lasting 123 Myr in the Tauris & Savonije (1999) model, as compared to 60 Myr in our calculations. This may be understood in terms of a different treatment of binary interactions (tides, magnetic braking, winds) as well as the difference in stellar models which may lead to a different starting point of RLOF.

8.1.6. *Long period NS-RG binary*

This RLOF sequence is taken from Tauris & Savonije (1999, their example 2c). We start with a 1.3 $\rm M_\odot$ NS + 1.0 $\rm M_\odot$ ZAMS star in a 60 day circular orbit. RLOF starts while secondary is on the RG branch ($t = 12312.5$ Myr since secondary ZAMS) and the binary is described by: $K_1 = 13$, $K_2 = 3$, $P_{\rm orb} = 60^d.708033$, $e = 0$, $M_1 = 1.3\ {\rm M}_\odot$, $M_2 = 0.98\ {\rm M}_\odot$, $R_1 = 0.000014\ {\rm R}_\odot$, and $R_2 = 30.5\ {\rm R}_\odot$. The evolution of the system during RLOF phase is shown in Figure 9.

RLOF is highly super-Eddington and driven by the expansion of the donor on a nuclear timescale. Only shortly

before the system detaches as a result of the exhaustion of the donor's envelope, the transfer rate becomes sub-Eddington. As a result, the donor loses most of its mass ($M_2 = 0.4$ M$_\odot$) while the NS hardly accretes any material ($M_1 = 1.43$ M$_\odot$). The orbit expands throughout this phase with the orbital period increasing to over 300 days. The system eventually forms a wide NS-He WD binary, with a potential recycled pulsar (the NS has accreted ~ 0.1 M$_\odot$).

The above results are very similar to the calculations of Tauris & Savonije (1999), who obtain a 1.5 M$_\odot$ NS with a 0.4 M$_\odot$ NS-He WD binary in a 382 day orbit. The mass transfer rates and duration of the RLOF phases are similar in both calculations.

8.1.7. *Long period NS-He star binary*

This RLOF sequence follows from Dewi & Pols (2003, see their Fig. 1). We start with a 1.4 M$_\odot$ NS + 2.8 M$_\odot$ ZAMS He star in a 10 day circular orbit. RLOF starts while the secondary is already an evolved He star (t = 2.9 Myr since the secondary He ZAMS) and the binary is described by: $K_1 = 13$, $K_2 = 8$, $P_{\rm orb} = 9^d.804617$, $e = 0$, $M_1 = 1.4$ M$_\odot$, $M_2 = 2.5$ M$_\odot$, $R_1 = 0.000014$ R$_\odot$, and $R_2 = 15.4$ R$_\odot$. The evolution of the system during RLOF phase is shown in Figure 10.

RLOF proceeds on the donor's thermal timescale throughout the entire phase. The very high mass transfer rate (6×10^{-3} M$_\odot$ yr^{-1}) makes this phase very short and RLOF stops after the envelope of He star is exhausted. Since the mass transfer rate is highly super-Eddington, the NS hardly accretes any material while the donor loses its entire He-rich envelope ($M_2 = 1.65$ M$_\odot$). The orbital period at first decreases to reach a minimum at 8.9 days, and then increases to 9.5 days at the end of RLOF phase. After the phase of RLOF the secondary core explodes in SN Ic leading to double neutron star formation (provided that a natal kick does not disrupt the binary). This result was presented also in Ivanova et al. (2003).

Dewi & Pols (2003) calculated a mass transfer rate spanning the range: 10^{-4}–10^{-2} M$_\odot$ yr^{-1}. Our rate is constant and close to the high end of the Dewi & Pols (2003) range. We have adopted a constant mass transfer rate following Paczynski (1971) who pointed out that thermal timescale mass transfer rates do not vary by more than factor of 2-3 (for details see § 5.3). This system may appear as an X-ray binary during this phase. However, the chances of catching it at this phase are very small, since the thermal timescale mass transfer is very short. Besides, in this case the X-rays may be significantly degraded because of high optical depths (material shed out of the system). On the other hand, some of these sources might appear to be γ-ray emitters with high intrinsic absorption, and the discovery of objects with these broad characteristics (see e.g., Dean et al. 2005) lends some hope for detecting this phase of binary evolution.

The results from Dewi & Pols (2003) reveal an opposite period evolution than in our simulation; it starts at higher value (10.36 days), growing to reach a maximum at 10.46 days and then decreasing to 10.37 days. However, the period changes in both calculations are rather small, and are probably related to our consistently high mass transfer rate throughout the RLOF phase. This leads to higher mass and angular momentum loss from the binary which determines the orbit evolution. Additionally, we include tidal interactions between binary components (see § 3.3 and § 8.2). These differences between the models for low mass helium stars were already noted by Dewi & Pols (2003).

8.1.8. *Short period NS-He star binary*

We choose this RLOF sequence from Dewi & Pols (2003, see their Fig. 3). We start with a 1.4 M$_\odot$ NS + 3.6 M$_\odot$ ZAMS He star in a 0.6 day circular orbit. RLOF starts while secondary is already an evolved He star (t = 2.0 Myr since the secondary He ZAMS) and the binary is described by: $K_1 = 13$, $K_2 = 8$, $P_{\rm orb} = 0^d.59$, $e = 0$, $M_1 = 1.4$ M$_\odot$, $M_2 = 3.2$ M$_\odot$, $R_1 = 0.000014$ R$_\odot$, and $R_2 = 2.4$ R$_\odot$. The evolution of the system during RLOF phase is shown in Figure 11.

RLOF proceeds on the donor's thermal timescale with a mass transfer rate of $\sim 10^{-3}$ M$_\odot$ yr^{-1} until the envelope of He star is almost exhausted. Since the mass transfer rate is highly super-Eddington, the NS does not accrete much material while the donor loses most of its He-rich envelope ($M_2 = 2$ M$_\odot$). The orbital period decreases from 0.6 to ~ 0.4 days at the end of RLOF phase. After the RLOF phase ceases the secondary explodes in SN Ib/Ic leading to a close double neutron star system (again provided that a natal kick does not disrupt the binary).

Dewi & Pols (2003) RLOF sequence for this case is very similar to our calculation. They find a period decrease (from 0.65 to 0.47 days) and a high constant mass transfer rate of a few $\times 10^{-4}$ M$_\odot$ yr^{-1}. The inspiral phase and CE is not expected in this case, and therefore further evolution may lead to a close double neutron star formation.

8.2. *Tidal Evolution Calibration*

Whenever coeval binary populations in nearby clusters are observed to constrain the circularization rate, it is found that standard tidal dissipation theories do not match the data (see Meibom & Mathieu 2005 for a recent review). In all cases an increase in the tidal dissipation rate appears necessary (Claret & Cunha 1997; Terquem et al. 1998). Depending on which theory is used, the increase needed in the overall efficiency of tidal dissipation is by a factor $\sim 10 - 100$.

We have used `StarTrack` models to calibrate our theoretical treatment by comparing them against observations of *(i)* the cutoff period for circularization in a population of MS binaries (in M67), and *(ii)* the orbital decay accompanying tidal synchronization in a high mass X-ray binary (LMC X-4). The results, presented in two following subsections, confirm that tidal dissipation is more effective than predicted by our simple theory. Therefore, in all our standard model calculations, we will use an increased rate of tidal dissipation, corresponding to $F_{\rm tid} = 10$ (see § 3.3 for our implementation of tidal dissipation theory and the definition of $F_{\rm tid}$), but we will also allow for even more effective tidal dissipation rates in our parameter studies (all the way to $F_{\rm tid} = 100$) .

8.2.1. *Cutoff Period for M67*

Open star clusters have often been used to test tidal interaction theories (Mathieu et al. 1992; Meibom & Mathieu 2005). Observations of single- and double-line spectro-

scopic binaries allow estimates of the periods and eccentricities for a number of systems within clusters. It was expected and then confirmed that the cutoff period ($P_{\rm cut}$, the longest period of a circular binary) should increase with the age of the cluster. The tidal dissipation depends strongly on the orbital separation and therefore the wider, longer-period binaries will take a greater time to circularize. In principle, with knowledge of the initial conditions in a given cluster, the observed value of the cutoff period may be used to calibrate the efficiency of tidal interactions. In practice, binaries within a given cluster form with eccentricities, separations and angular momenta which are not precisely known. In addition, the observed samples may suffer from small number statistics (the observed cutoff periods are only lower limits), rendering such a calibration quite uncertain. However, we can use the cutoff-period observations to provide at least an order of magnitude estimate for the factor by which any standard theoretical estimate must be increased.

M67 is an old open cluster with an age of 3.98 Gyr and observed cutoff period of $10-12$ d (Mathieu, Latham & Griffin 1990; Mathieu et al. 1992) and a solar metallicity stellar population (Janes & Phels 1994). The period was estimated for a sample of MS binaries with components close to the cluster turnoff mass. Recently Meibom & Mathieu (2005) proposed a new way to estimate the point of transition from circular to eccentric systems. Instead of a simple cutoff period, they use a new estimator called the "tidal circularization period." This period is found from fitting a special function which mimics the tidal circularization isochrone of the most frequently occurring eccentric binary orbits for a given cluster. They find that the tidal circularization period for M67 is 12.1 d.

Several calculations, with different efficiencies of tidal dissipation, were performed to try to reproduce the binary population of the open cluster M67. In each calculation we have evolved 10^4 binaries at solar metallicity with component masses in the $0.7-1.4$ $M_\odot$ range, requiring that the mass ratio be greater than 0.5. The limits are somewhat arbitrary, but chosen to include the population of bright MS stars observed in M67. The initial distributions were chosen as in our standard evolutionary model (see § 5.7), but with IMF exponent $\alpha_{\rm imf}=2.35$, which is more appropriate for clusters (Kroupa & Weidner 2003).

In Figure 12 we show synthetic binary MS populations in the period–eccentricity plane corresponding to an evolution with different efficiencies for the tidal interaction. As expected we see that the cutoff period increases for more efficient tidal interactions, $P_{\rm cut}\simeq 4,7,10$ d for $F_{\rm tid}=1,10,100$, respectively. It is found that only for significantly increased dissipation ($F_{\rm tid}\gtrsim 10-100$) the predicted cutoff period approaches the observed value of 10-12 days. One additional calculation with $F_{\rm tid}=1000$ results in a cutoff period of ~ 16 days, now clearly higher than the observed value.

8.2.2. *Orbital decay of LMC X-4*

Levine, Rappaport & Zojcheski (2000) measured the orbital period decay for the high mass X-ray binary (HMXB) LMC X-4. The system consists of a 1.3 $M_\odot$ NS and a massive 15.6 $M_\odot$ companion in a 1.4-day circular or almost circular orbit (Woo et al. 1996; van der Meer et al. 2005). The X-ray emission in HMXBs is believed to arise from wind accretion onto the compact object; however it was also suggested that some systems may be in an atmospheric RLOF phase (e.g., Kaper 2001). For wind-fed detached systems, the orbital decay may be directly connected to the tidal interaction of the HMXB components. The rotation of the massive component decreases with time as it expands during the evolution. The tidal forces act to try to synchronize the massive component, resulting in loss of orbital energy and angular momentum, i.e., decay of the orbit.

If, in fact, LMC X-4 is a wind-fed system, i.e., not in RLOF, then the massive star must be smaller than its Roche lobe $R_{\rm roche}=8$ $R_\odot$. A 15.6 $M_\odot$ star exceeds that size, while still on MS, after about 10.5 Myr of evolution (from the ZAMS). Subsequent RLOF is dynamically unstable (extreme mass ratio) and leads to a rapid merger of the binary components, terminating the HMXB phase. We perform a set of calculations for a synthetic binary similar to the LMC X-4 using our standard model parameters, with the metallicity appropriate for the LMC ($Z=0.007$). We *assume* that the binary configuration is detached and we calculate the rate of orbital decay. The results are shown in Figure 13 for various efficiencies of tidal interactions ($F_{\rm tid}=1,10,100$). The orbital decay rate increases with time as the massive component expands along the MS and approaches its Roche lobe. The time to reach contact (at which point calculations are stopped) decreases with increasing effectiveness of tidal forces. For comparison we show the observed orbital decay for LMC X-4, which falls within a model with moderately increased tidal interactions efficiency ($F_{\rm tid}=10$).

However, the orbital decay rate depends crucially on the current relative radius of the massive component of LMC X-4 ($\propto (R/a)^8$, see eq. 13). The calculations shown in Figure 13 correspond to the massive MS star at 8 Myr (after the ZAMS) with a radius of $\simeq 6.5-7$ $R_\odot$. If the calculations were started at a later age when the star was larger, say about 8 $R_\odot$ (almost filling its Roche lobe), then it would be possible to reproduce the observed orbital decay with weaker tidal dissipation ($F_{\rm tid}\sim 1$). The orbital decay measurements with the associated error on the stellar radius ($R\simeq 6.8-8.5$ $R_\odot$; Woo et al. 1996) are consistent with both small and intermediate values of our $F_{\rm tid}$ calibration factor. We also find that we cannot reproduce the observed decay rate with $F_{\rm tid}\gtrsim 100$ for any radius within observational errors (a good match is then found only if the massive component radius is <5.8 $R_\odot$).

9. X-RAY MODELING

9.1. *X-ray luminosity calculations*

In our study we consider only accreting binaries with NS and BH primaries, which are brighter than some X-ray luminosity cut $L_{\rm x,cut}$. This cut may correspond to a detection limit of a particular set of observations. Typical $L_{\rm x,cut}$ values for most current *Chandra* observations are in the range $10^{34}-10^{36}$ erg s^{-1}. At these high luminosities in the Chandra sensitivity range ($\sim 0.3-7$ keV) the only WD accretors will be supersoft sources, which are easily identifiable from their X-ray spectra and are thought to have most of their X-ray emission coming from nuclear burning rather than gravitational energy release (see Kuulkers et al. 2003 for a review of the X-ray properties of WD

accretors). Although, for some deep Galactic exposures *Chandra* has reached levels of $\sim 10^{30}$ erg s^{-1} (e.g., Galactic Center image of Muno et al. 2003) and a contribution from cataclysmic variables may also become important. The calculation of X-ray luminosities of systems with WD accretors will be described in a separate study (Ruiter, Belczynski & Harrison 2005, in preparation).

Binary companions to NS/BHs may lose material either through a stellar wind or via RLOF. In the latter case, the donors transfer all the material toward the accretor, whereas for the wind-fed systems only a fraction of the material is captured by the compact object. We calculate the bolometric luminosity ($L_{\rm bol}$) arising from the accretion onto a compact object. The accretion rate is based on the secular averaged mass accretion rate. If a system is detached then we use the wind mass accretion rate (eq. 29), and if system is semi-detached the RLOF accretion rate is used (eq. 45). We do not calculate X-ray luminosities arising from the accretion in dynamically unstable phases, since the timescales are very short and additionally X-ray emission would be highly absorbed due to large optical depths in the CE. The $L_{\rm bol}$ is calculated from

$$L_{\rm bol} = \epsilon \frac{G M_{\rm acc} \dot{M}_{\rm acc}}{R_{\rm acc}} \qquad (77)$$

where the radius of the accretor is 10 km for a NS and 3 Schwarzschild radii for a BH, and ϵ gives a conversion efficiency of gravitational binding energy to radiation associated with accretion onto a NS (surface accretion $\epsilon = 1.0$) and onto a BH (disk accretion $\epsilon = 0.5$).

For RLOF-fed systems we make a distinction between persistent and transient X-ray sources. All wind-fed systems are considered as persistent X-ray sources. The issue of the wind-fed XRBs with massive B*e* companions and their outburst behavior is discussed in § 9.2.

RLOF-fed systems are subject to a thermal disk instability and may appear either as persistent or transient X-ray sources depending on the mass transfer rate. A system becomes a transient X-ray source when the RLOF rate falls below a certain critical value $\dot{M}_{\rm disk}$. We use the work of Dubus et al. (1999) for H-rich disks (see their eq.30) and the study of Menou, Perna, & Hernquist (2002) for disks with heavier elements (see their eqs.1–4)

$$\dot{M}_{\rm disk} = \begin{cases} 1.5\times10^{15} M_{\rm acc}^{-0.4} R_{\rm disk}^{2.1} C_1^{-0.5} g s^{-1} & H-rich \\ 5.9\times10^{16} M_{\rm acc}^{-0.87} R_{\rm disk}^{2.62} \alpha_{0.1}^{0.44}\ g s^{-1} & He-rich \\ 1.2\times10^{16} M_{\rm acc}^{-0.74} R_{\rm disk}^{2.21} \alpha_{0.1}^{0.42}\ g s^{-1} & CO-rich \\ 5.0\times10^{16} M_{\rm acc}^{-0.68} R_{\rm disk}^{2.05} \alpha_{0.1}^{0.45}\ g s^{-1} & O-rich, \end{cases} \qquad (78)$$

where $M_{\rm acc}$ is accretor mass in $M_\odot$, $R_{\rm disk}$ is a maximum disk radius (2/3 of accretor Roche lobe radius) in 10^{10} cm. Constants are: $C_1 = C/(5\times10^{-4})$, with C being radiation constant of typical value 5×10^{-4}); $\alpha_{0.1} = \alpha/0.1$, with α being a viscosity parameter. Following Menou et al. (1999) we adopt $\alpha = 0.1$ for all types of donors since there is empirical evidence from dwarf nova outbursts that this is the right order of magnitude for the viscosity parameter. The same value of α is used to derive the critical mass transfer rate for H-rich disks (Dubus et al. 1999). H-rich donors are the stars with types $K_{\rm i} = 0, 1, 2, 3, 4, 5, 6, 16$, He-rich donors are $K_{\rm i} = 7, 8, 9, 10, 17$, CO-rich donors are $K_{\rm i} = 11$, while we apply formulae for O-rich type donors to ONe WDs ($K_{\rm i} = 12$).

We adopt a semi-empirical approach to calculate quiescent X-ray luminosities of transient NS RLOF-fed sources, since little is known about the emission mechanism during quiescence. It is not certain if the emission arises from a low level accretion or a deep crustal heating (for a detailed discussion see Belczynski & Taam 2004b, and references therein). Using X-ray studies of Galactic transient systems with NS accretors (e.g., Tavani & Arons 1997; Rutledge et al. 2001; Campana & Stella 2003; Jonker, Wijnands & van der Klis 2004; Tomsick et al. 2004; Campana 2004), we adopt 10^{31} erg s^{-1} as a lower limit for the hard X-ray luminosity, above 2 keV. However, it was shown that the average luminosity level can be higher $\gtrsim 10^{32}$ erg s^{-1} (e.g., Rutledge et al. 2002; Jonker et al. 2004). We adopt an X-ray luminosity level of $10^{31} - 10^{32}$ erg s^{-1} above 2 keV. Furthermore, we assume that the quiescent NS transient X-ray luminosities are evenly distributed in the above range.

The quiescent emission from BH transient systems is likely related to a low level of mass accretion. Recent observations of BH transients in their quiescent states (Tomsick et al. 2003) reveal rather hard spectra that are not well described by a black body. The observed luminosities are found in the range $\sim 10^{30} - 10^{33}$ erg s^{-1} with a median luminosity $\simeq 2\times10^{31}$ erg s^{-1}. For BH systems we also use a semi-empirical approach, and we assume that most (80%) of the quiescent BH transient X-ray luminosities above 2 keV are evenly distributed in the $10^{30} - 10^{32}$ erg s^{-1} range, while the rest (20%) of the systems are slightly brighter: luminosities evenly distributed in the $\sim 10^{32} - 10^{33}$ erg s^{-1} range (see Fig. 3 of Tomsick et al. 2003). There are some indications that the highest quiescent luminosities are found in the longest period systems (e.g. Garcia et al. 2001), but we do not implement this effect until more observations are available.

RLOF-fed transient systems in outburst reach high (close to Eddington) X-ray luminosities. We introduce a factor η_{out} describing the fraction of the critical Eddington luminosity a given system has reached. The long period systems, with orbits that are sufficiently extensive for a large accretion disk to be formed, are usually found to emit at the Eddington luminosity ($L_{\rm edd}$) during outburst, while the outburst luminosities of short period systems are lower by about an order of magnitude. The correction factor to an X-ray luminosity at outburst corresponding to $\eta_{\rm out} = 0.1$ and $\eta_{\rm out} = 1$ for the short and long period systems is applied respectively. The critical periods, over which the Eddington luminosity is adopted, are taken to be 1 day and 10 hrs for NS and BH transients in outburst, respectively (Chen, Shrader & Livio 1997; Garcia et al. 2003; see also appendix A1 in Portegies Zwart, Dewi & Maccarone 2004).

In order to decide if a given transient system is in an active (outburst) state or inactive (quiescent) state we need to know the disk duty cycle ($DC_{\rm disk}$). However, the disk instability theory cannot provide a reliable estimate of $DC_{\rm disk}$. Empirically it is thought that $DC_{\rm disk} \lesssim 1\%$

(e.g., Taam, King & Ritter 2000). We adopt $DC_{\rm disk} = 1\%$ (probability of finding a system in outburst) in our calculations and use Monte Carlo to decide the state of a transient system. In practice when we study a stellar population we extract the information for all X-ray binaries at some specified time (time slice). Once we decide that a given system is a transient (see eq. 78) we draw a random number (flat probability distribution) from the range 0–1. If the number is smaller than 0.01 (1% probability) the system is then in outburst, otherwise it is in quiescence. The appropriate X-ray luminosity is then assigned to the system (see eq. 80). Alternatively, we use a phenomenological model for the duty cycle developed by Portegies Zwart et al. 2004. The model is based on the observations available for the Galactic BH transient systems. In particular comparison of the recurrence time and the decay time combined with the observed peak outburst energy allows to calculate the time in which system is brighter than a certain critical X-ray luminosity. Specific application of that model will be discussed in the forthcoming paper on the evolution of X-ray luminosity function in starburst galaxies (Belczynski et al. 2006, in preparation).

Finally, the bolometric accretion luminosity is converted to an X-ray luminosity in a specific energy range. We perform the conversion to the 0.3 – 7 keV range, which may be used directly for comparison with *Chandra* observations. For all the persistent RLOF-fed sources, all wind-fed sources and the transients in the outburst stage, where accretion is the dominant contributor to the observed luminosity, we apply a bolometric correction ($\eta_{\rm bol}$). For all quiescent transients the bolometric correction is not needed since we adopted their X-ray luminosities directly from observations. For different types of systems we estimate the correction to be:

$$\eta_{\rm bol} = \begin{cases} 0.15 & \text{NS : wind : all} \\ 0.55 & \text{NS : RLOF : pers., outburst trans.} \\ 0.8 & \text{BH : wind : all} \\ 0.8 & \text{BH : RLOF : pers., outburst trans.} \end{cases} \quad (79)$$

Corrections were obtained from: La Barbera et al. (2001) for wind-fed NS systems; from Di Salvo et al. (2002) and Maccarone & Coppi (2003) for RLOF-fed NS systems; and from Miller et al. (2001) for BH systems. These bolometric corrections will be applicable for the typical *Chandra* observations of external galaxies. For deeper observations, where the lower luminosity cutoffs are below a few percent of the Eddington limit, the objects make spectral state transitions (see Maccarone 2003 and references within), and the bolometric corrections are much larger[2].

Combining all of the above information, we can calculate the X-ray luminosity of synthetic X-ray binaries from

$$L_{\rm x} = \begin{cases} 10^{31} - 10^{32} & \text{all quiescent NS transients} \\ 10^{30} - 10^{32} & \text{80\% quiescent BH transients} \\ 10^{32} - 10^{33} & \text{20\% quiescent BH transients} \\ \eta_{\rm bol}\eta_{\rm out}L_{\rm edd} & \text{outburst NS/BH transients} \\ \eta_{\rm bol}L_{\rm bol} & \text{persistent (RLOF and wind)} \end{cases} \quad (80)$$

where $L_{\rm x}$ is expressed in erg s^{-1} and $L_{\rm edd}$ represents the Eddington luminosity.

9.2. *High Mass X-ray Binaries: Be Star Transients*

9.2.1. *Observational Overview*

High mass X-ray binaries (HMXBs) consist of a compact object (either a NS or a BH) orbiting a massive star. Both galactic and extra-galactic populations of HMXBs are known (Liu, van Paradijs & van den Heuvel 2000, 2005). The majority of HMXBs (about 2/3; see Liu et al. 2000, 2005; Hayasaki & Okazaki 2005) are so-called Be/X-ray binaries, in which the primary is a Be star, orbited by a magnetized NS. Orbits are generally wide with a moderate eccentricity. The compact star accretes from the wind of a massive main sequence or subgiant Be (spectral types B3-O with Balmer emission lines; Zorec & Briot 1997) companion. Many of these systems show transient behavior (see below). The remaining HMXBs are those in which the primary is a supergiant, so called SG/X-ray binary (e.g., Liu et al. 2000). For these systems the compact object either accretes from the wind of the supergiant, or in brighter systems through RLOF via an accretion disk.

Some Be/X-ray binaries (B*e* XRBs) are persistent sources (varying by less then a factor of ~ 10) observed at low luminosity levels $L_{\rm x} \sim 10^{32} - 10^{34}$ erg sec^{-1} (e.g., Van Bever & Vanbeveren 2000; Okazaki & Negueruela 2001). However, most B*e* XRBs show periodic outbursts and are called transient B*e* XRBs. Transient B*e* XRBs exhibit two different types of outbursts (e.g., Bildsten et al. 1997; Okazaki & Negueruela 2001; Hayasaki & Okazaki 2005; Baykal et al. 2005):

– Type I (normal) outbursts, which are of moderate intensity ($L_{\rm x} \sim 10^{36} - 10^{37}$ erg sec^{-1}) and they appear to be related to the orbital period. It is generally accepted that these outbursts are associated with the periastron passage of a NS, and are explained by the increased accretion from the B*e* star wind at periastron.

– Type II (giant) outbursts, with luminosities reaching $L_{\rm x} \gtrsim 10^{37}$ erg sec^{-1}, are irregular, and although they seem to appear shortly after the periastron passage, they do not exhibit any other correlations with an orbital period. Although the origin of the Type II outbursts remains unknown, it was suggested that the outflow from the B*e* star may lead to the formation of a transient accretion disk around the NS. Disk accretion results in higher X-ray luminosities than direct surface wind accretion (see Bildsten et al. 1997 for a discussion and references). Some systems show both types of outbursts, e.g., A 0535+262 (Motch et al. 1991; Finger, Wilson & Harmon 1996), V0332+53 (Stella, White & Rosner 1986) or 4U 0115+634 (Baykal et al. 2005).

9.2.2. *Modeling*

Type I outbursts are averaged out of our calculations if we use the orbit-averaged wind accretion model (see § 4.2). In the general (arbitrary eccentricity) wind accretion model (see § 4.1) Type I outbursts are a natural outcome. However, it was noted (Avni & Goldman 1980) that the transient phenomenon may be then hard to explain.

We construct a simple phenomenological model for Type II outbursts in order to be able to assess the influence of this transient activity on XRB population characteristics.

[2]However, note that the quiescent X-ray luminosities are not affected since they are adopted directly from the deep observations.

For a system to be a potential Type II B*e* XRB outburster we require:
– a binary with a NS or a BH accretor and a massive MS ($K_{\rm i} = 1$) or subgiant ($K_{\rm i} = 2$) donor ($M \geq 8$ M$_\odot$, spectral type earlier than B3),
– that the system is tight enough so it appears as a HMXB with a persistent (outside outbursts) wind accretion leading to an X-ray luminosity greater than $L_{\rm x,Be}$. We allow $L_{\rm x,Be}$ to change within the range $10^{32} - 10^{34}$ erg sec^{-1}.

Furthermore, only a fraction ($f_{\rm Be}$) of donors in the above binaries are B*e* stars (as opposed to a regular B stars), and can potentially trigger the Type II outbursts. To provide an upper limit on the contribution of bursting HMXBs to the XRB population one may choose $f_{\rm Be} = 1$. For detail studies, the $f_{\rm Be}$ may be constrained based on the age of a massive star (McSwain & Gies 2005) or its spectral type and luminosity class (Zorec & Briot 1997). Little is known about the duty cycle of Type II outbursts, we therefore allow the duty cycle to change within a wide range $DC_{\rm Be} = 0.1 - 0.5$ and use Monte Carlo to decide whether the system is in outburst or in quiescence. $DC_{\rm Be}$ gives the fraction of a time a given system spends in the outburst. We use an orbit averaged X-ray luminosity (direct wind accretion) for the quiescence ($\eta_{\rm bol} = 0.15, 0.8$ § 9.1), although thermal emission from a NS is also observed in some systems. For systems in the Type II outburst the X-ray luminosity is taken to be uniformly distributed in the range $L_{\rm x} = 10^{37} - 10^{38}$ erg sec^{-1}. We adopt bolometric correction factors: $\eta_{\rm bol} = 0.15, 0.8$ for NS and BH accretors, respectively (see § 9.1).

The X-ray modeling will be further developed as we proceed with the studies of the Galactic and extragalactic X-ray binary populations (e.g., Belczynski et al. 2006, in preparation).

10. SUMMARY

We have presented a detailed description of the updated `StarTrack` population synthesis code. The code is being used to study populations of different varieties of binaries hosting compact objects. The code has been calibrated and tested against different sets of observations and detailed evolutionary calculations and the results are presented here. The updated version of `StarTrack` was already used in several studies of compact object binaries and XRBs. `StarTrack` allows for evolution of stellar systems with a wide variety of different initial conditions (IMF, metallicity, star formation history) and for a number of different evolutionary models, subject to the parameterizations of the input physics.

In a series of papers that will follow we will address the issues of modeling of XRBs, and will focus on the comparison of synthetic XRB populations with the observed X-ray point source populations in nearby galaxies. The code is also being used to study populations of binaries with NSs and BHs as potential source candidates for ground based interferometric gravitational radiation observatories (e.g., GEO, LIGO, VIRGO) as well as populations of less-massive WD binaries for space-based projects (e.g., LISA).

Although a number of physical processes governing single and binary evolution remain highly uncertain, the advances in observational techniques and new results of massive surveys allow now various aspects of stellar evolution to be explored. We have incorporated several different evolutionary models within `StarTrack` (e.g., different magnetic braking laws or CE prescriptions) making possible tests of their validity. For example, one such test may be based on a comparison of synthetic and observed X-ray luminosity functions for nearby starburst galaxies.

The `StarTrack` code described in this paper may be used only for the evolution of isolated stars and binaries, i.e., in stellar systems in which dynamical interactions are not important (e.g., field populations, open clusters). However, a number of interesting studies may be carried out for dense stellar environments, in which both stellar evolution and dynamical interactions play an important role in the formation of compact object binaries. In particular, `StarTrack` was integrated with a dynamical code for these types of studies (for details see Ivanova et al. 2005).

We would like to thank R.Webbink, G.Nelemans, T. Di Salvo and A.Ruiter for useful discussions and comments on the manuscript. KB and TB acknowledge partial support through KBN Grant 1 P03D 022 28. VK acknowledges support through a David and Lucile Packard Foundation Fellowship in Science and Engineering and through NASA grants NAG5-13056 and NAS8-03060. This research was supported in part by the NSF under Grant No. AST-0200876 to RT.

REFERENCES

Abramowicz, M.A., Czerny, B., Lasota, J.P., & Szuszkiewicz, E. 1988, ApJ, 332, 646
Abt, H. A. 1983, ARA&A, 21, 343
Andronov, N., Pinsonneault, M., & Sills, A. 2003, ApJ, 582, 358
Arzoumanian, Z., Chernoff, D. F., & Cordes, J. M. 2002, ApJ, 568, 289
Avni, Y., & Goldman, I. 1980, A&A, 90, 44
Bailyn, C.D., & Grindlay, J.E. 1990, ApJ, 353, 159
Baykal, A., Kiziloglu, U, Kiziloglu, N., Balman, S., & Inam, S.C. 2005, A&A, 439, 1131
Begelman, M.C., 2002, ApJ, 568, L97
Belczynski, K., Benacquista, M., Larson, S., & Ruiter, A. 2005a, ApJ, submitted (astro-ph/0510718)
Belczynski, K., Bulik, T., & Kalogera, V. 2002a, ApJ571, L147
Belczynski, K., Bulik, T., & Rudak, B. 2002b, ApJ, 571, 394
Belczynski, K., Bulik, T., & Ruiter, A. 2005b, ApJ, 629, 915
Belczynski, K., & Kalogera, V. 2001, ApJ, 550, L183
Belczynski, K., Kalogera, V., & Bulik, T. 2002c, ApJ, 572, 407 (BKB02)
Belczynski, K., Kalogera, V., Zezas, A., & Fabbiano, P. 2004a, ApJ, 601, L147
Belczynski, K., Sadowski, A., & Rasio, F. 2004b, ApJ, 611, 1068
Belczynski, K., Sadowski, A., Rasio, F., & Bulik, T. 2005c, ApJ, submitted (astro-ph/0508005)
Belczynski, K., & Taam, R. E. 2004a, ApJ, 603, 690
Belczynski, K., & Taam, R. E. 2004b, ApJ, 616, 1159
Bildsten, L., et al. 1997, ApJS, 113, 367
Bleach, J.N. 2002, MNRAS, 332, 689
Blecha, L., Ivanova, N., Kalogera, V., Belczynski, K., Fregeau, J., & Rasio, F. 2005, ApJ, submitted (astro-ph/0508597)
Blondin, J. M. 1986, ApJ, 308, 755
Boffin, H.M.J., & Jorissen, A. 1988, A&A, 205, 155
Bondi, H., & Hoyle, F. 1944, MNRAS, 104, 273
Brown, G.E. 1995, ApJ, 440, 270
Campana, S. 2005, in Binary Radio Pulsars, ASP Conference Series Vol. 328 (eds. F. A. Rasio & I. Stairs), 432
Campana, S., & Stella, L. 2003, astro-ph/0309811
Chevalier, R. A. 1989, ApJ, 346, 847
Chevalier, R. A. 1993, ApJ, 411, L33
Chen, W., Shrader, C.R., & Livio, M. 1997, ApJ, 491, 312

Claret, A., & Cunha, N.C.S. 1997, A&A, 318, 187
Cordes, J., & Chernoff, D.F. 1998, ApJ, 505, 315
Dean, A.J., et al., 2005, A&A, in press, (astro-ph/0508291)
Dewi, J.D.M., & Pols, O.R. 2003, MNRAS, 344, 629
Dewi, J. D. M., & Tauris, T. M. 2000, A&A, 360, 1043
Di Salvo, T., et al. 2002, A&A, 386, 535
Dubus, G. et al. 1999, MNRAS, 303, 139
Duquennoy, A., & Mayor, M. 1991, A&A, 248, 485
Finger, M.H., Wilson, R.B., & Harmon, B.A. 1996, ApJ, 459, 288
Fox, D.B., et al. 2005, Nature, 437, 845
Fryer, C., Burrows, A., & Benz, W. 1998, ApJ, 496, 333
Garcia, M.R., McClintock, J.E., Narayan, R., Callanan, P., Barret, D., & Murray, S.S. 2001, ApJ, 553, L47
Garcia, M.R., Miller, J.M., McClintock, J.E., King, A.R., & Orosz, J. 2003, ApJ, 591, 388
Garcia-Senz, D., Bravo, E., & Woosley, S.W. 1999, A&A, 349, 177
Gilfanov, M., 2004, MNRAS, 349, 146
Goldreich, P., & Keeley, D.A. 1977, ApJ, 211, 934
Grimm, H.-J., Gilfanov, M., Sunyaev, R. 2003, MNRAS, 339, 793
Hachisu, I., Kato, M., & Nomoto, K. 1999, ApJ, 522, 487
Hashimoto, M.A., Nomoto, K.I., Arai, K., & Kaminisi, K. 1986, ApJ, 307, 687
Hayasaki, K., & Okazaki, A.T. 2005, MNRAS, submitted (astro-ph/0503066)
Heggie, D. C. 1975, MNRAS, 173, 729
Hjellming, M.S. 1989, Ph.D. Thesis, University of Illinois
Hjellming, M.S., & Webbink, R.F. 1987, ApJ, 318, 794
Hobbs, G., Lorimer, D.R., Lyne, A.G., & Kramer, M. 2005, MNRAS, 360, 974
Hurley, J. R., Pols, O. R., & Tout, C. A. 2000, MNRAS, 315, 543
Hurley, J. R., Tout, C. A., & Pols, O. R. 2002, MNRAS, 329, 897
Hut, P. 1981, A&A, 99, 126
Hut, P., & Paczynski, B. 1984, ApJ, 284, 675
Ihm, M., Kalogera, V., & Belczynski, K. 2005, ApJ, submitted (astro-ph/0508626)
Ivanova, N. 2006, ApJ, in press (astro-ph/0509514)
Ivanova, N., Belczynski, K., Fregeau, J.M., & Rasio, F.A. 2005, MNRAS, 358, 572
Ivanova, N., Belczynski, K., Kalogera, V., Rasio, F., & Taam, R. E. 2003, ApJ, 592, 475
Ivanova, N., & Taam, R. E. 2003, ApJ, 599, 516
Ivanova, N., & Taam, R. E. 2004, ApJ, 601, 1058
Janes, K.A., & Phels, R.L. 1994, AJ, 108, 1773
Jonker, P. G., Wijnands, R., & van der Klis 2004, MNRAS, 349, 94
Kalogera, V., & Webbink, R. 1996, ApJ, 458, 301
Kalogera, V. 1996, ApJ, 471, 352
Kaper, L. 2001, in Proceedings of "Influence of binaries on stellar population studies", ed. Vanbeveren, Kluwer Acad. Pub., p. 125
Kato, M., & Hachisu, I. 1999, ApJ, 513, L41
Kato, M., & Hachisu, I. 2004, ApJ, 613, L129
Kim, D.-W., & Fabbiano, G. 2004, ApJ, 611, 846
King, A. R., & Begelman, M. C. 1999, ApJ, 519, L169
de Kool, M. 1990, ApJ, 358, 189
Kroupa, P., Tout, C.A., & Gilmore, G. 1993, MNRAS, 262, 545
Kroupa, P., & Weidner, C. 2003, ApJ, 598, 1076
Kuiper, G. P. 1935, PASP, 47, 15
Kuulkers, E., Norton, A., Schwope, A., & Warner, B. 2003, to appear in Compact Stellar X-ray Sources, Cambridge University Press, eds. W.H.G. Lewin and M. van der Klis
La Barbera, A., Burderi, L., Di Salvo, T., & Robba, N.A. 2001, ApJ, 553, 375
Lai, D., Rasio, F.A., & Shapiro, S.L. 1993, ApJS, 88, 205
Levine, A., Rappaport, S.A., & Zojcheski, G. 2000, 541, L194
Liu, Q.Z., van Paradijs, J., & van den Heuvel, E.P.J. 2000, A&AS, 147, 25
Liu, Q.Z., van Paradijs, J., & van den Heuvel, E.P.J. 2005, A&A, 442, 1135
Maccarone, T.J., 2003 A&A, 409, 697
Maccarone, T.J., & Coppi, P.S. 2003, A&A, 399, 1151
Mathieu, R. D., Duquennoy, A., Latham, D. W., Mayor, M., Mermilliod, T., & Mazeh, J. C. 1992, Proceedings of "Binaries as Tracers of Stellar Formation", ed. Duquennoy, A. & Mayor, M., Cambridge University Press, p.278
Mathieu, R. D., Latham, D. W., & Griffin, R. F. 1990, AJ, 100, 1859
McSwain, M.V., & Gies, D.R. 2005, ApJS, accepted (astro-ph/0505032)
van der Meer, A., Kaper, L., Van Kerkwijk, M.H., & Van den Heuvel, E.P.J. 2005, in the proceedings of the International Workshop "Massive Stars in Interacting Binaries, submitted (astro-ph/0502313)
Meibom, S., & Mathieu, R.D. 2005, ApJ, 620, 970
Menou, K., Perna, R., & Hernquist, L. 2002, ApJ, 564, L81
Meurs, E.J.A., & van den Heuvel, E.P.J. 1989, A&A, 226, 88
Miller, J.M., Fox, D.M., Di Matteo, T., Wijnands, R., Belloni, T., Pooley, D., Kouvelioutou, C., & Lewin, W.H.G. 2001, ApJ, 546, 1055
Motch, C., Stella, L., Janot-Pacheco, E., & Mouchet, M. 1991, ApJ, 369, 490
Muno, M.P., et al. 2003, ApJ, 589, 225
Nieuwenhuijzen, H., & de Jager, C. 1990, A&A, 231, 134
Nelemans, G., & Tout, C. A. 2005, MNRAS, 356, 753
Nutzman, P., Kalogera, V., Finn, L.S., Hendrickson, C., & Belczynski, K. 2004, ApJ, 612, 364
Okazaki, A.T., & Negueruela, I. 2001, A&A, 377, 161
O'Shaughnessy, R., Kalogera, V., & Belczynski, K. 2005a, ApJ, 620, 3850
O'Shaughnessy, R., Kaplan, J., Kalogera, V., & Belczynski, K. 2005b, ApJ, 632, 1025
O'Shaughnessy, R., Kim, C., Frakgos, T., Kalogera, V., & Belczynski, K. 2005c, ApJ, 633, 1076
Paczynski, B. 1971, ARA&A, 9, 183
Paczynski, B., & Ziolkowski, J. 1967, Acta Astronomica, 17, 7
Peters, P. C. 1964, Phys.Rev., 136, B1224
Pfahl, E.D., Rappaport, S., & Podsiadlowski, Ph. 2002a, ApJ, 571, L37
Pfahl, E.D., Rappaport, S., Podsiadlowski, Ph., & Spruit, H. 2002b, ApJ, 574, 364
Podsiadlowski, P., Joss, P.C., & Hsu, J.J.L. 1992, ApJ, 391, 246
Podsiadlowski, P., Langer, N., Poelarends, A.J.T., Rappaport, S., Heger, A., & Pfahl, E.D. 2004, ApJ, 612, 1044
Portegies Zwart, S.F., Dewi, J., & Maccarone, T. 2004, MNRAS, 355, 413
Prialnik, D., & Kovetz, A. 1995, ApJ, 445, 789
Rappaport, S., Verbunt, F., & Joss, P.C. 1983, ApJ. 275, 713
Rasio, F.A., Tout, C.A., Lubov, S.H., & Livio, M. 1996, ApJ, 470, 1187
Ritter, H. 1999, MNRAS, 309, 360
Rutledge, R. E., Bildsten, L., Brown, E. F., Pavlov, G. G., & Zavlin, V. E. 2001, ApJ, 559, 1054
Rutledge, R. E., Bildsten, L., Brown, E. F., Pavlov, G. G., & Zavlin, V. E. 2002, ApJ, 577, 346
Saio, H., & Nomoto, K. 1998, ApJ, 500, 388
Savonije, G.J., de Kool, M., & van den Heuvel, E.P.J. 1986, A&A, 155, 51
Stauffer, J.B., & Hartmann, L.W. 1986, PASP, 98, 1233
Stella, L., White, N.E., & Rosner, R. 1986, ApJ, 308, 669
Taam, R.E. 1980, ApJ, 242, 749
Taam, R.E., King, A.R., & Ritter H. 2000, ApJ, 541, 329
Tauris, T.M., & Savonije, G.J. 1999, A&A, 350, 928
Tauris, T. M. & Takens, R. J. 1998, A&A, 330, 1047
Tavani, M., & Arons, J. 1997, ApJ, 477, 439
Terquem, C., Papaloizou, J.C.B., Nelson, R.P., & Lin, D.N.C. 1998, ApJ, 502, 788
Theuns, T., Boffin, H.M.J., & Jorissen, A. 1996, MNRAS, 280, 1264
Tomsick, J.A., et al. 2003, ApJ, 597, L133
Tomsick, J. A., Gelino, D. M., Halpern, J. P., & Kaaret, P. 2004, ApJ, in press
Wang, Q.D., Gotthelf, E.V., & Lang, C.C. 2002, Nature, 415, 148
Wellstein, S., & Langer, N. 1999, A&A, 350, 148
Wellstein, S., Langer, N., & Braun, H. 2001, A&A, 369, 939
Webbink, R. F. 1984, ApJ, 277, 355
Willems, B., & Kolb, U. 2003, MNRAS, 343, 949
Woo, J.W., et al. 1996, ApJ, 467, 811
Van Bever, J., & Vanbeveren, D. 2000, A&A, 358, 462
Vanbeveren, D., Van Rensbergen, W., & De Loore, C. 1998, in 'The Brightest Binaries", Astrophysics and Space Science Library, Vol. 232, p. 124
Zahn, J.P. 1975, A&A, 41, 329
Zahn, J.P. 1977, A&A, 57, 383; erratum 67, 162
Zahn, J.P. 1989, A&A, 220, 112
Zangrilli, L., Tout, C.A., & Bianchini, A. 1997, MNRAS, 289, 59
Zorec, J., & Briot, D. 1997, A&A, 318, 443

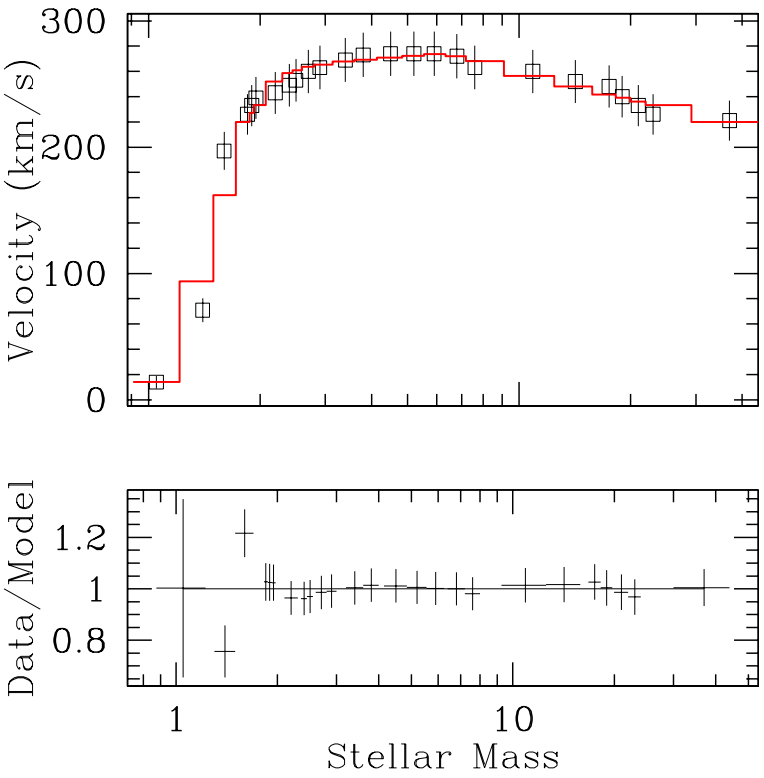

Fig. 1.— Initial rotational velocities of stars used in `StarTrack` calculations. In the top panel we present the fit to the observational data from Stauffer & Hartmann (1986). In the bottom panel we show the ratio of the data and the model.

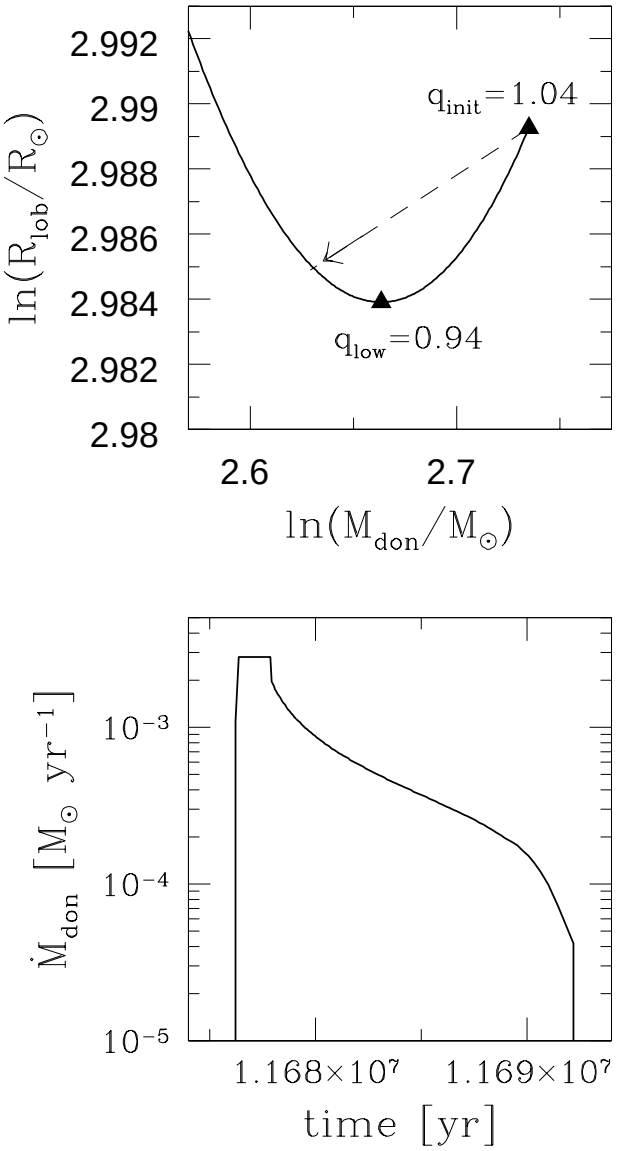

Fig. 2.— The diagnostic diagram (top panel) used to decide whether a binary should be evolved on a thermal timescale or rather RLOF is dynamically unstable (leading to CE evolution and a potential merger). If the mass ratio at the onset of RLOF ($q_{\rm int}$) is much greater than the mass ratio at the moment when the orbit starts expanding ($q_{\rm low}$) then the system is dynamically unstable, otherwise RLOF on a thermal timescale is assumed. The arrow represents the partial derivative of donor radius (equal to the Roche lobe radius) with respect to its mass, and points to the place where the donor is expected to regain thermal equilibrium. The bottom panel shows a specific system: a 16 $M_\odot$ Hertzsprung Gap donor with a 15 $M_\odot$ MS companion in an 8-day orbit, for which the diagnostic diagram is plotted. The mass transfer begins on a thermal timescale (flat part) and then evolves on a slower nuclear timescale (decline). For more details see § 5.2.

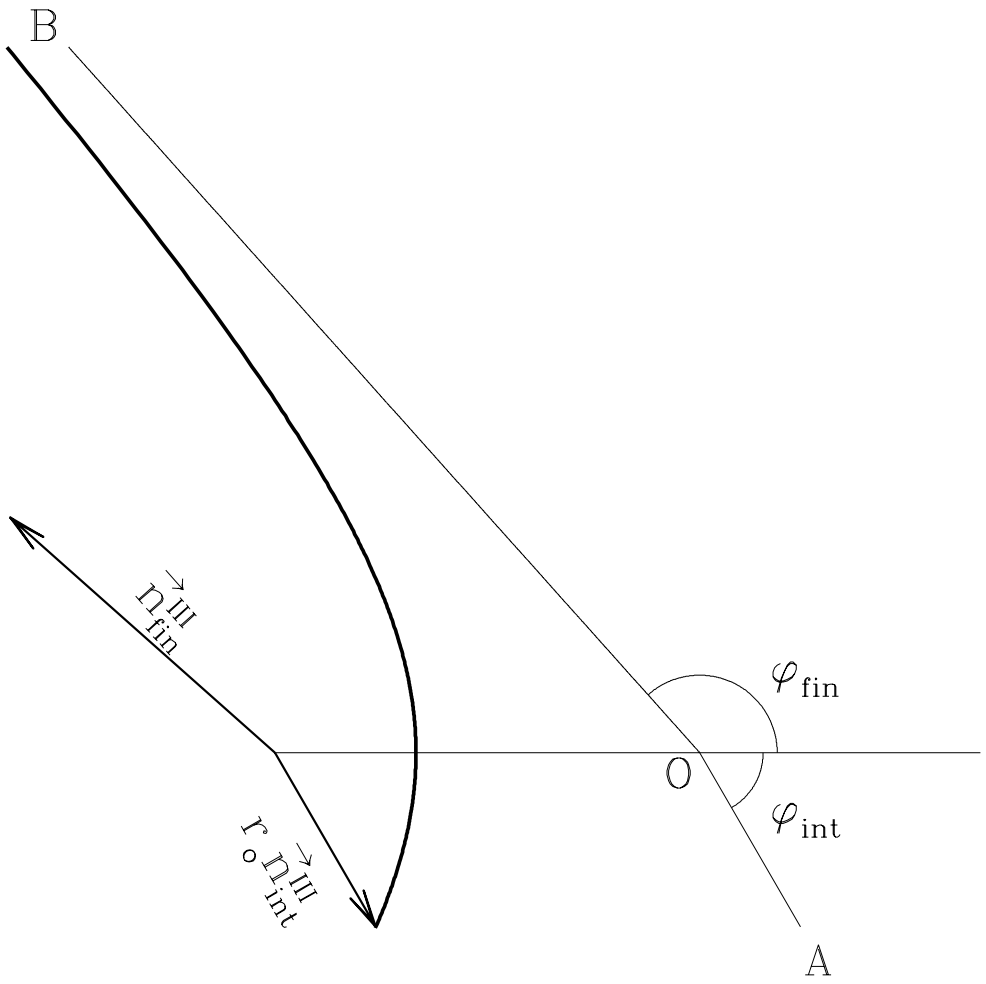

Fig. 3.— The case of a binary disrupted in a supernova explosion: we present the orbit in the coordinate system III (for details see § 6). The line OA is parallel to the vector $\vec{n}^{III}_{\rm int}$, while the line OB, the asymptote of the hyperbola, is parallel to the vector $\vec{n}^{III}_{\rm fin}$. The point O is the focus of the hyperbola.

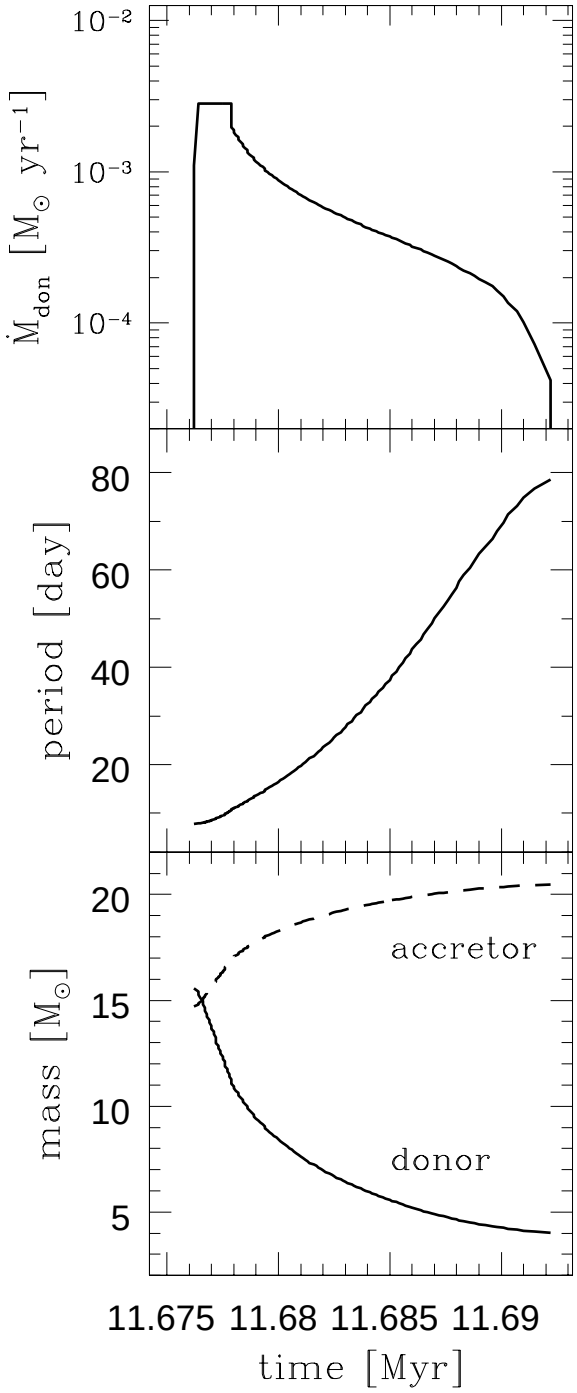

Fig. 4.— RLOF sequence for 16 $M_\odot$ HG + 15 $M_\odot$ MS binary. Top panel shows mass transfer rate, middle panel orbital period, while bottom panel component mass evolution during RLOF phase.

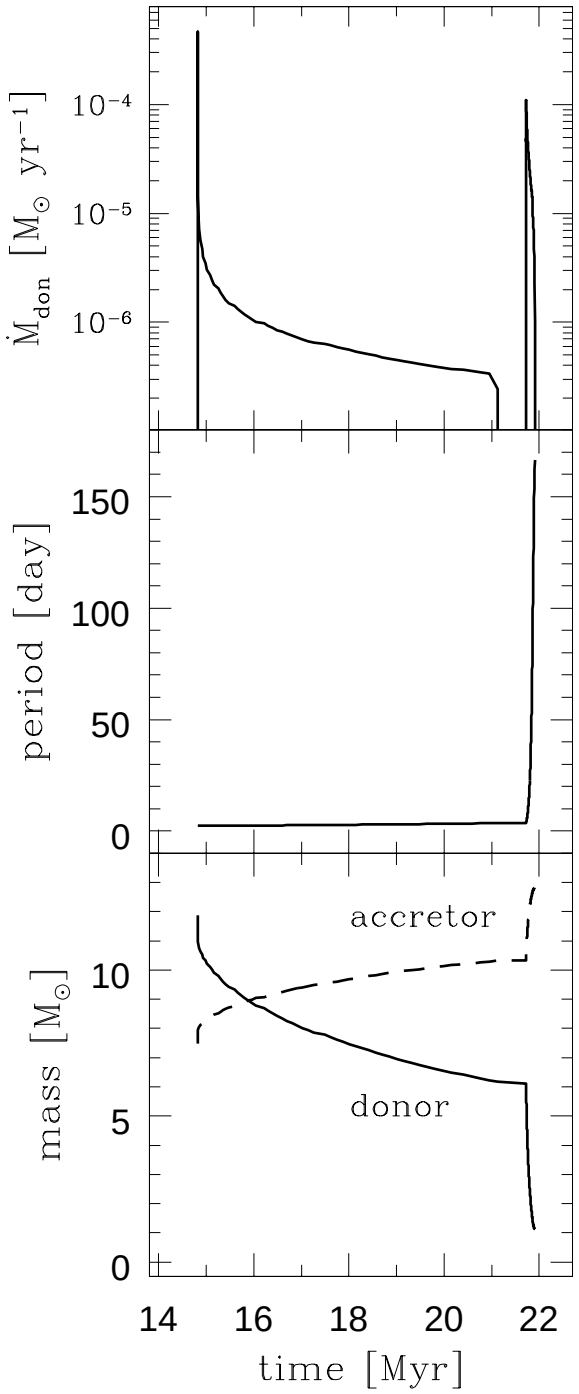

Fig. 5.— RLOF sequence for 12 $M_\odot$ MS + 7.5 $M_\odot$ MS binary. Panels same as in Fig. 4.

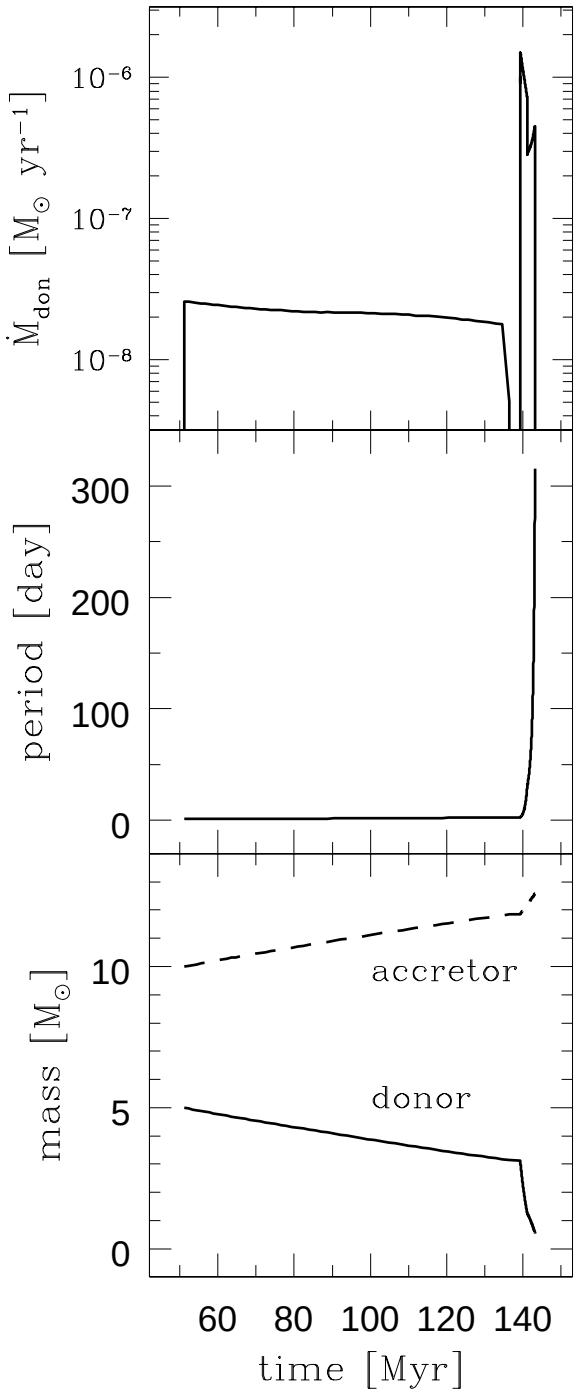

Fig. 6.— RLOF sequence for 10 $M_\odot$ BH + 5 $M_\odot$ MS binary. The critical Eddington mass accretion rate onto the BH is about $3.1 - 4 \times 10^{-7}$ $M_\odot$ yr^{-1}. Panels same as in Fig. 4.

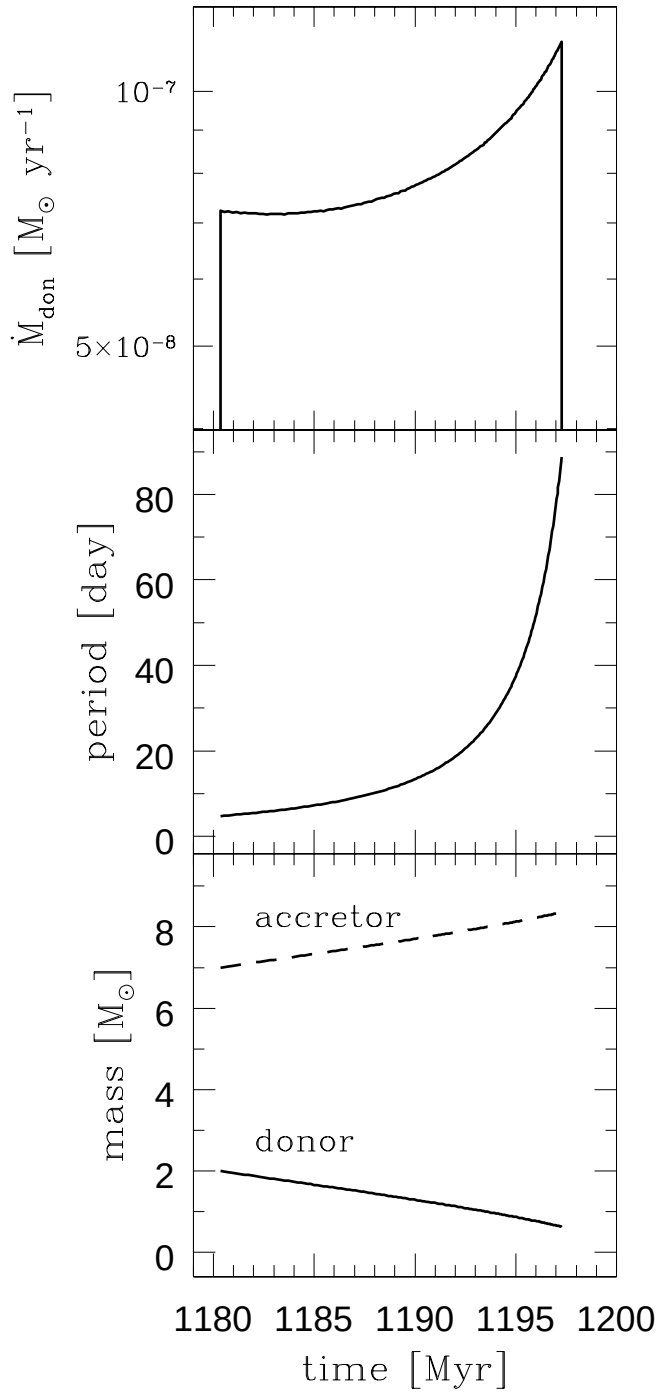

Fig. 7.— RLOF sequence for 7 $M_\odot$ BH + 2 $M_\odot$ RG binary. The critical Eddington mass accretion rate onto the BH is about $2.2 - 2.6 \times 10^{-7}$ $M_\odot$ yr^{-1}. Panels same as in Fig. 4.

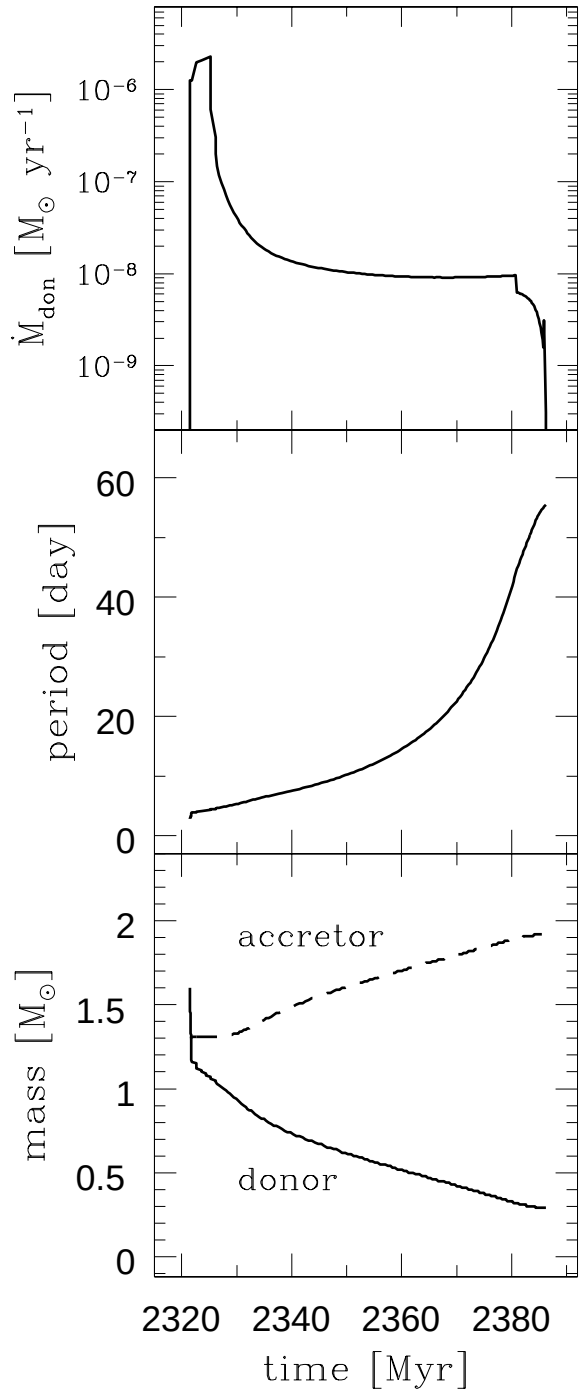

Fig. 8.— RLOF sequence for 1.3 $M_\odot$ NS + 1.6 $M_\odot$ RG binary. The critical Eddington mass accretion rate onto the NS is $\sim 1.7 \times 10^{-8}$ $M_\odot$ yr^{-1}. Panels same as in Fig. 4.

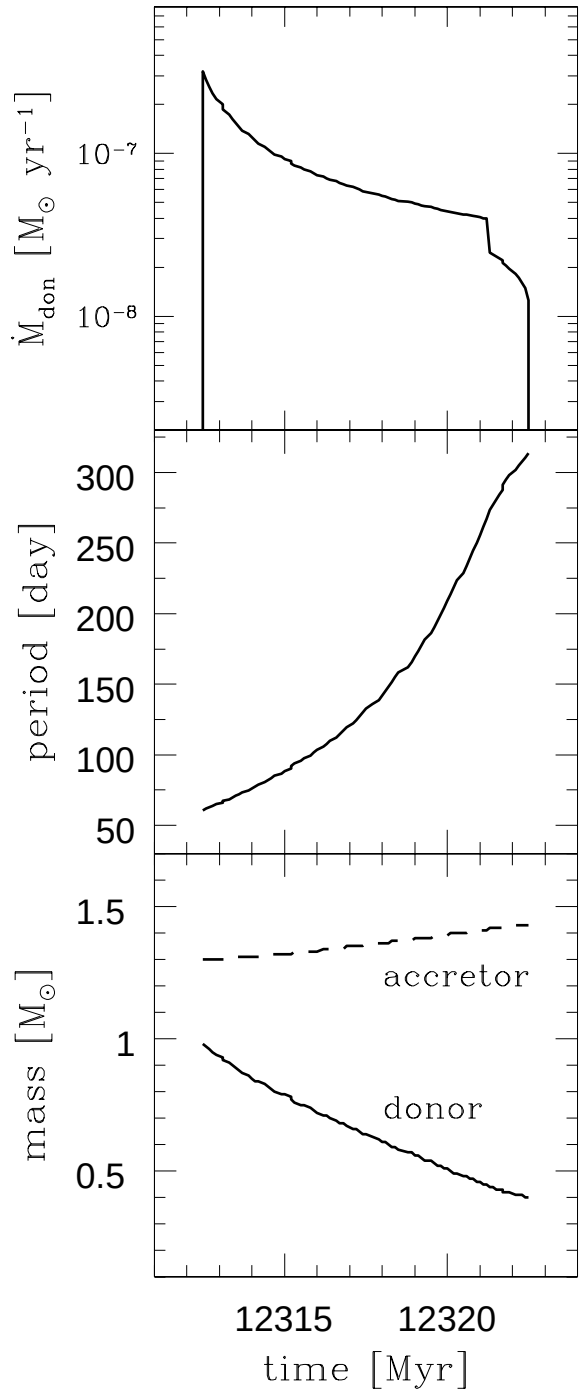

Fig. 9.— RLOF sequence for 1.3 $M_\odot$ NS + 1 $M_\odot$ RG binary. The critical Eddington mass accretion rate onto the NS is $\sim 1.7 \times 10^{-8}$ $M_\odot$ yr^{-1}. Panels same as in Fig. 4.

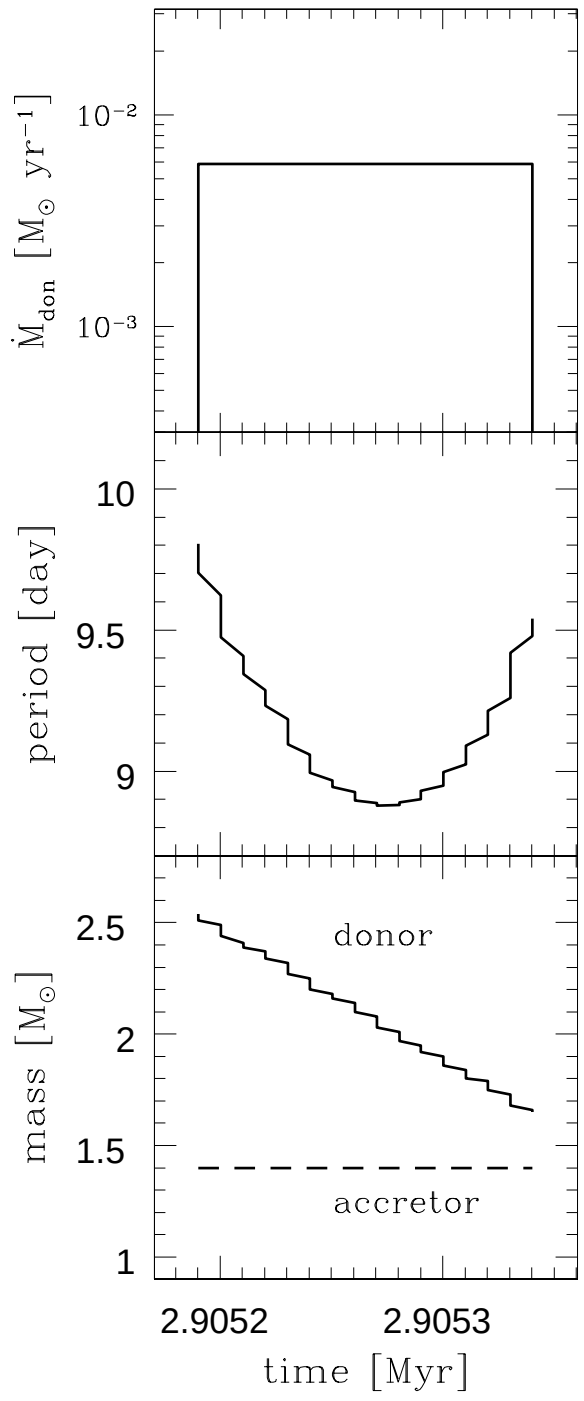

Fig. 10.— RLOF sequence for 1.4 $M_\odot$ NS + 2.8 $M_\odot$ evolved He-star binary. The critical Eddington mass accretion rate onto the NS is $\sim 2.9 \times 10^{-8}$ $M_\odot$ yr^{-1}. Panels same as in Fig. 4. Note the very short duration of this RLOF phase; the (finite) timesteps taken by the code may be seen through lines showing orbital period and donor mass.

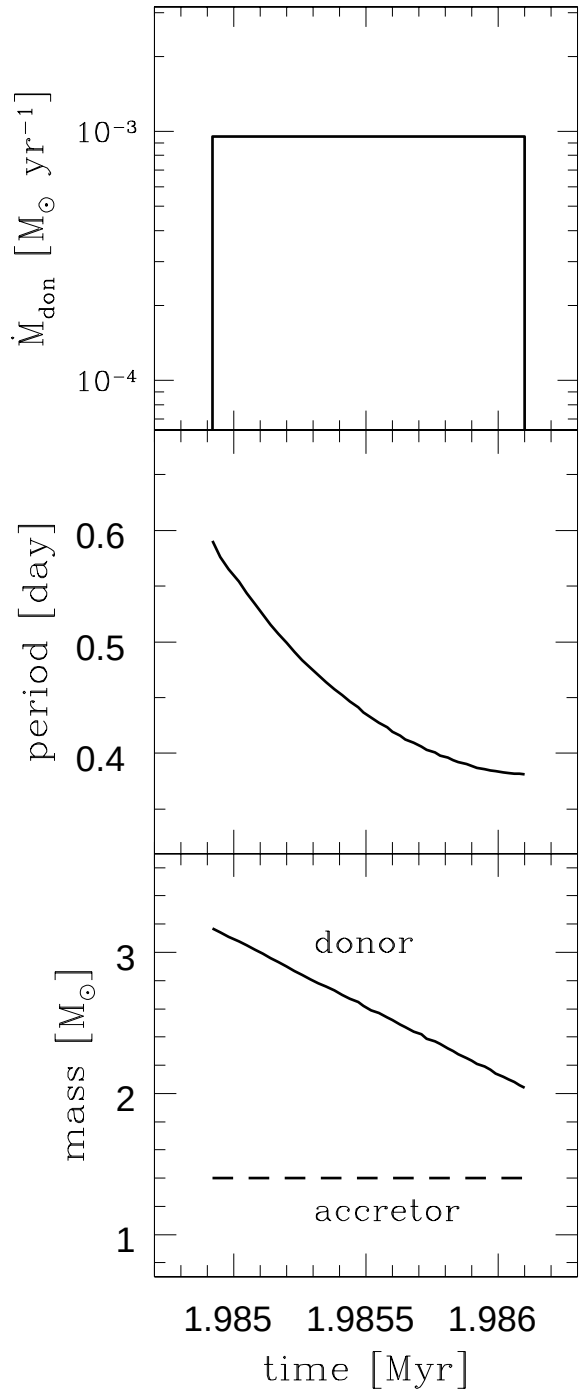

Fig. 11.— RLOF sequence for 1.4 $M_\odot$ NS + 3.6 $M_\odot$ evolved He-star binary. The critical Eddington mass accretion rate onto the NS is $\sim 2.9 \times 10^{-8}$ $M_\odot$ yr^{-1}. Panels same as in Fig. 4.

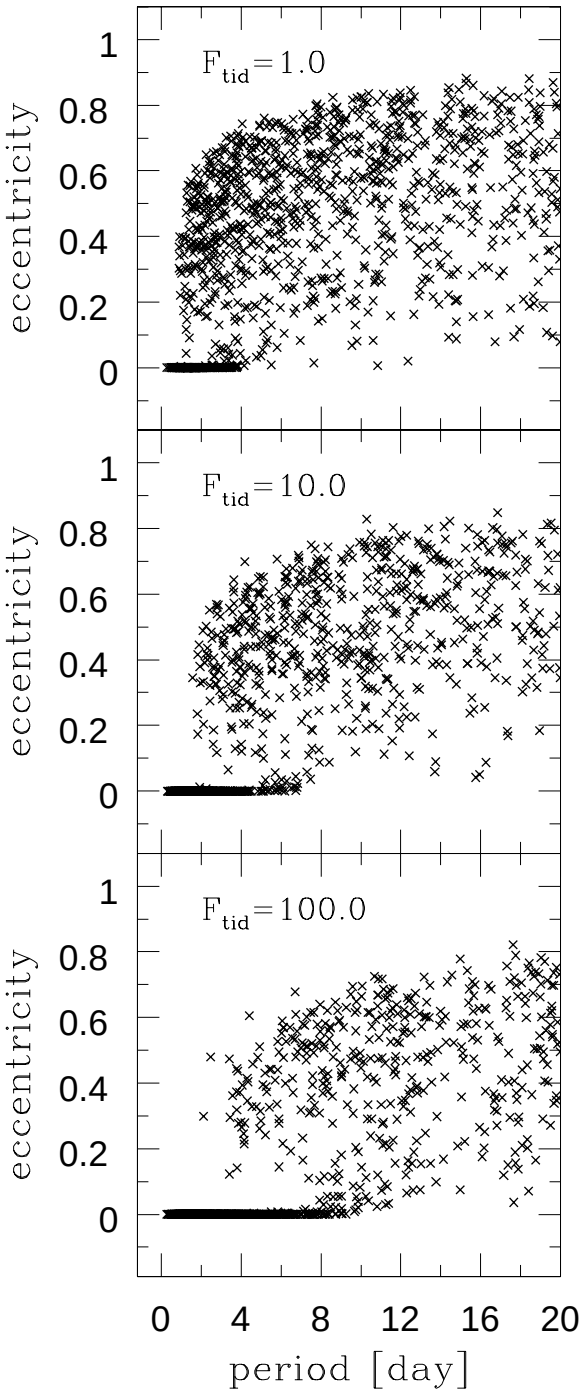

Fig. 12.— Tidal calibration calculation for the open cluster M67. The figure shows the period–eccentricity plane with the population of main sequence binary stars at 3.98 Gyr, the current age of the cluster. Bottom and middle panels show the results of evolution with increased tidal interactions ($F_{\rm tid} = 100, 10$, respectively) as opposed to the standard prescription, presented on the top panel ($F_{\rm tid} = 1$). Note the increase of cutoff period (the longest period circular binary in a given sample) with increasing $F_{\rm tid}$. The observed cutoff period for M67 is $P_{\rm cut} \simeq 10 - 12$ days. For more details see § 8.2.1.

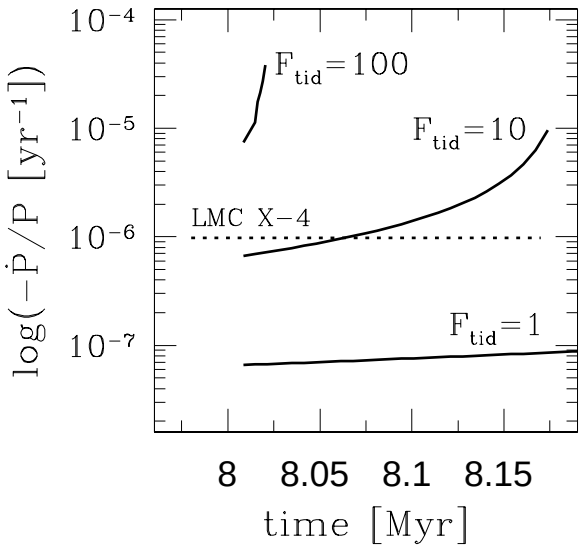

Fig. 13.— Tidal calibration calculation for the high-mass X-ray binary LMC X-4. The observed orbital decay rate for LMC X-4 is $-9.8\times10^{-7}\mathrm{yr}^{-1}$ (marked with dotted line). Predicted decay rates for different efficiencies of tidal interactions ($F_{\rm tid} = 100, 10, 1$) are shown with solid lines. For more details see § 8.2.3.